Nanoscale

Accepted Manuscript

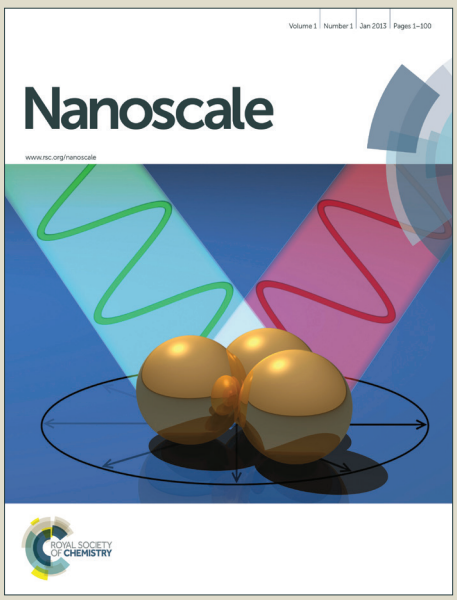

ROYAL SOCIETY OF CHEMISTRY

www.rsc.org/nanoscale

Cite this: DOI: 10.1039/c0xx00000x

www.rsc.org/xxxxxx

Review

Graphitic carbon nitride based nanocomposites: A review

Zaiwang Zhao [a], Yanjuan Sun [a], Fan Dong [a*]

[a] Chongqing Key Laboratory of Catalysis and Functional Organic Molecules, College of Environmental and Biological Engineering, Chongqing Technology and Business University, Chongqing, 400067, China.

Received (in XXX, XXX) Xth XXXXXXXXX 20XX, Accepted Xth XXXXXXXXX 20XX
DOI: 10.1039/b000000x

Abstract: Graphitic carbon nitride (g-C_3N_4), as an intriguing earth-abundant visible light photocatalyst, possesses a unique two-dimensional structure, excellent chemical stability and tunable electronic structure. Pure g-C_3N_4 suffers from rapid recombination of photo-generated electron-hole pairs resulting in low photocatalytic activity. Because of the unique electronic structure, the g-C_3N_4 could act as an eminent candidate for coupling with various functional materials to enhance the performance. According to the discrepancies in photocatalytic mechanism and process, six primary systems of g-C_3N_4-based nanocomposites can be classified and summarized**.** Namely, the g-C_3N_4 based metal-free heterojunction, g-C_3N_4/single metal oxide (metal sulfide) heterojunction, g-C_3N_4/composite oxide, g-C_3N_4/halide heterojunction, g-C_3N_4/noble metal heterostructures, and g-C_3N_4 based complex system. Apart from the depiction of fabrication methods, heterojunction structure and multifunctional application of the g-C_3N_4-based nanocomposites, we emphasize and elaborate on the underlying mechanisms in the photocatalytic activity enhancement of g-C_3N_4-based nanocomposites. The unique functions of p–n junction (semiconductor/semiconductor heterostructures), the Schottky junction (metal/semiconductor heterostructures), the surface plasmon resonance (SPR) effect, photosensitization, super conductivity, etc., are utilized in the photocatalytic processes. Furthermore, the enhanced performance of g-C_3N_4-based nanocomposites has been widely employed in environmental and energetic applications such as photocatalytic degradation of pollutants, photocatalytic hydrogen generation, carbon dioxide reduction, disinfection, and super capacitor. This critical review ends with a summary and some perspectives on the challenges and new directions in exploring g-C_3N_4-based advanced nanomaterials.

∗ To whom correspondence should be addressed. Email: dfctbu@126.com (F. Dong).
Tel.: +86-23-62769785-605; Fax: +86-23-62769785-605.

Cite this: DOI: 10.1039/c0xx00000x

www.rsc.org/xxxxxx

Review

1. Introduction

Over the past decades, the growing awareness of environmental protection and energy conservation has stimulated intensive research on solar energy utilization.[1] In the domain of pollutants elimination and solar energy conversion, semiconductor photocatalysis has emerged as one of the most fascinating technologies[2-5]. Nevertheless, the wide band gap and low solar-energy utilization efficiency remain the "bottleneck" of the photocatalysts to satisfy the requirement of applications in a practical way. For instance, the traditional TiO_2 is limited for its poor performances associated with visible light application. As a result, it is urgent to seek for efficient visible-light-driven (VLD) photocatalysts. For this objective, various modified TiO_2 and TiO_2-alternative photocatalysts have been fabricated.[6-17] Currently, it is still a challenge to design new photocatalysts that are abundant, stable and facile in fabrication besides high visible-light performance.

In the search for robust and stable VLD semiconductor photocatalysts, a polymeric semiconductor, graphitic carbon nitride (g-C_3N_4), has recently attracted tremendous attention. The heptazine ring structure and high condensation degree enable metal-free g-C_3N_4 to possess many advantages such as good physicochemical stability, as well as an appealing electronic structure combined with a medium-band gap (2.7 eV).[18] These unique properties make g-C_3N_4 a promising candidate for visible light photocatalytic applications utilizing solar energy. In addition, g-C_3N_4 is abundant and easily-prepared via one-step polymerization of cheap feedstocks like cyanamide,[18,19] urea,[20-22] thiourea,[23,24] melamine [25-27] and dicyandiamide.[28,29] Nevertheless, pure g-C_3N_4 suffers from shortcomings such as rapid recombination of photo-generated electron-hole pairs, small specific surface area and low visible light utilization efficiency.[21-29] Consequently, the exploration of facile and dependable strategies to synthesize the modified g-C_3N_4-based photocatalysts with improved physicochemical properties and high photocatalytic activities is of increasing requirement. The g-C_3N_4 has a unique two-dimensional layered structure, which is favorable for hybridizing with other components. Very recently, several approaches have been employed to enhance the visible light photocatalytic performance of g-C_3N_4, such as formation of surface coupling hybridization utilizing TaON,[30] Bi_2WO_6,[31] graphene,[32] construction of mesoporous structure,[33] doping with metal or nonmetal species Fe,[34] Ag,[35] Au,[36] Pd,[37] S,[38] B[39] and P[40] and sensitizing by organic dyes.[41] Among these approaches, formation of heterostructures demonstrates a great potential to promote the photocatalytic performance of g-C_3N_4 because the electron–hole pairs can be efficiently separated, and charge carriers could transfer across the interface of the heterostructure to restrain the recombination.

In a coupling process, g-C_3N_4 based heterostructures not only can be formed by combining with visible light excited photocatalytic semiconductor materials with a narrow band gap such as CdS,[42] Bi_2WO_3,[43] BiOI[44]), but also can combine with UV excited photocatalysts with large band gap (such as as TiO_2,[45] ZnO,[46] $ZnWO_4$[47]), which can largely broaden the application of the g-C_3N_4 based nanocomposites. Neverthess, not all materials can couple with g-C_3N_4 to form a heterostructures. The most important prerequisite condition to form an effective visible light excited g-C_3N_4 based heterostructure is that the candidates should have an appropriate band structure which is beneficial to create a coupling hybridization. Besides, the difference of chemical potential between the coupling semiconductor A and B generates band bending at the interface of junction. The band bending induces a built-in field, which impels the photogenerated electrons and holes to transfer in opposite directions, resulting in a spatially efficient separation of the electrons and holes pairs on different sides of heterojunction.[48,49] In addition, the crystal structure in the junction domain of the heterostructure is also important in strengthening the quantum efficiency of the photocatalyst. A distinction in lattice spacing between two semiconductors could probably cause lattice mismatch. The lattice mismatch at the interface may cause defects, which will capture the photo-generated electronic carriers and thus inhibit the diffusion of electrons and holes. Thus, the formation of g-C_3N_4 based heterostructures is an effective approach to enhance charge separation efficiency for improved photocatalytic performance.

Recently, numerous researches have been made to couple g-C_3N_4 with various semiconductors to enhance the photocatalytic activities.[36,50-51] For instances, Wang and co-workers firstly reported TiN/g-C_3N_4 multi-layers hybridization by using a dual-facing-target magnetron sputtering method at room temperature, and exhibited favorable properties in photocatalytic applications in 2008.[50] This pioneering work has stimulated tremendous interests on the fabrication, modification, and application of g-C_3N_4-based semiconductor photocatalysts. Yan et al. successfully developed g-C_3N_4/TaON organic–inorganic composite photocatalyst with visible-light response by a milling-heat treatment method that demonstrated an enhanced photocatalytic performance for photodegradation of Rhodamine B (RhB) in aqueous solutions.[51] Di et al. prepared the Au/g-C_3N_4 nanocomposites photocatalyst by depositing gold nanoparticles on the surface of a g-C_3N_4 semiconductor to generate metal–semiconductor junctions, which showed well-improved photocatalytic hydrogen evolution with visible light.[36]

Now that significant advances have been made on the g-C_3N_4-based photocatalysts in recent years, we believe that a comprehensive review on this subject is necessary to accelerate further developments in this exciting research domain. This review article is focused on recent progress in the design, fabrication, mechanistic understanding, and the potential applications of these g-C_3N_4-based nanocomposites in various realms such as photodegradation of nitrogen oxides, organic contaminants photodegradation, photocatalytic hydrogen evolution, conversion carbon dioxide to methane fuel, oxygen reduction reaction (ORR), and photoelectrochemical

determination of Cu^{2+} . Eventually, some concluding remarks and invigorating perspectives on the current situation and further prospects on the g-C_3N_4-related researches are presented, which may promote the understanding and large scale application of the g-C_3N_4-based nanocomposites.

2. g-C_3N_4-based nanocomposites

2.1 Preparation of g-C_3N_4

Generally, carbon nitride materials fabricated by directly condensation of nitrogen-containing organic precursors (for example urea, thiourea, melamine, dicyandiamide, cyanamide, guanidine hydrochloride) are bulk materials with a small surface area, normally below 10 m^2/g. For practical applications of the materials in domains such as a single catalyst or a support substrate of co-catalysts (such as heterojunction), the introduction of well-controlled porosity at the nanoscale in the bulk carbon nitride is mandatory to strengthen its utilizations to a large scale. And it is worth noting that formation of mesoporous and augment of specific surface area are crucial to fine-tune the physicochemical properties and improve the photocatalytic performance.[52] As previously reported, the mesoporous g-C_3N_4 (mpg-C_3N_4) was firstly obtained by nanocasting/replication of mesoporous silica matrices, which were famous for the generation of the corresponding carbon nanostructures.[53,54,55] Inspired by this hard template method, tremendous attempts were stimulated to explore new strategies for g-C_3N_4 modification, such as soft template method,[56-58] ultrasonic dispersion method,[59] acidic solution impregnation[60,61] and chemical functionalization.[62-66] As universally applied, methods mentioned above were good as a proof-of-principle in tailoring the texture and surface chemical properties, as well as the electronic properties.

2.2 Design considerations for g-C_3N_4-based nanocomposites

To develop effective g-C_3N_4-based nanocomposites working for enhanced performance, several pivotal requirements must be considered. First of all, the semiconductor light harvesting antenna must have a narrow band gap to allow for efficient absorption of the solar spectrum. Second, there must be a driving force boosting charge separation and accelerating the transportation process. Furthermore, the semiconductor should possess adequate redox potential for the desired photochemical reactions. Ultimately, a mechanism should be accompanied to guarantee the photochemical stability of the photocatalyst. It is unlikely that a single material system could satisfy all these requirements, while the nanocomposites photocatalysts may have the potential to accomplish these goals. In general, nanocomposites photocatalysts could offer several potential merits: (1) Cocatalyst effect. The integration with a proper cocatalyst can lower the redox overpotential at the respective active sites; (2) Strengthened light absorption. For instance, semiconductors with small band gap possessing high absorption coefficiency can be utilized to functionalize (or sensitize) semiconductor materials with large band gaps; (3) Efficient charge separation and transportation. A p-n (semiconductor/semiconductor heterostructures) or the Schottky junction (metal/semiconductor heterostructures) with built-in electrical potential can be constructed in heterogeneous photocatalysts to effectively expedite electron-hole pair separation and transportation; (4) Decent stability. If the active sites and function groups on the semiconductor surface can be protected through proper surface passivation, it is possible to improve the stability.

In consideration of the diverse mechanisms of different g-C_3N_4 based nanocomposites in photocatalytic reactions, g-C_3N_4 based heterojunctions were summarized and classified into six main different combination systems. Below we review the recent progress on the g-C_3N_4 based metal-free heterojunction, g-C_3N_4/metal oxide (metal sulfide) heterojunction, g-C_3N_4/inorganic acid salts composites, g-C_3N_4/halide heterojunction, g-C_3N_4/noble metal heterostructures, and g-C_3N_4 based multi-component heterojunction for improved photocatalysis.

3. Categories of g-C_3N_4 based nanocomposites

3.1 g-C_3N_4 based metal-free layered heterojunction

To our knowledge, metal-free materials owing to various advantages such as low-cost and environmentally amicable, have stimulated multitudinous attention because of their great potential in solving environmental and energy problems. Hence, it is extremely attractive to construct hybridized materials via coupling two metal-free materials. For example, graphene, a two-dimensional macromolecular sheet of carbon atoms, has preferentially attracted much attention due to its outstanding mechanical, thermal, easily-obtained, and electrical properties. And it has been widely used in nanoelectronics, biosensing, capacitors, and catalysis domains.[67,68] In particular, it possesses an extremely high specific surface area (~2600 m^2/g)[69] and marvelous thermal conductivity (~5000 W $m^{-1}K^{-1}$), guaranteeing a superb mobility of charge carriers (200 000 cm^2 $V^{-1}s^{-1}$). Therefore, the merits mentioned above made graphene as the first metal-free candidate, and preferentially used to construct layered graphene/g-C_3N_4 nanocomposites Sun et al prepared graphene/g-C_3N_4 nanoheterojunction by absorption-calculation method, which demonstrated apparently enhanced conductivity and electrocatalytic performance on oxygen reduction reaction (ORR).[70] Xiang et al also successfully obtained graphene/g-C_3N_4 nanocomposites by a combined impregnation-chemical reduction strategy, and firstly utilized this graphene/g-C_3N_4 nanoheterojunction in visible-light photocatalytic H_2-production containing Pt as a cocatalyst.[32] Fig. 1a and 1b show a typical TEM image of graphene oxide and graphene/g-C_3N_4 nanocomposites. In comparison to graphene oxide, the graphene/g-C_3N_4 composite possessed a more compact structure due to the fact that g-C_3N_4 was sandwiched between graphene sheets through polymerization of melamine molecules pre-adsorbed on the GO sheets. In the aforementioned trials, the high H_2-production activity over the graphene/g-C_3N_4 nanocomposites under visible-light irradiation can be achieved. The mechanism of the acvitiy enhancement is illustrated in Fig. 1c.

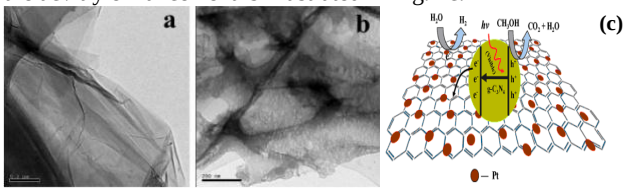

Fig. 1 (a) TEM images of graphene oxide and (b) the graphene/g-C_3N_4 nanocomposites; (c) Proposed mechanism for the enhanced electron transfer in the graphene/g-C_3N_4 composites (reprinted with permission from ref. 32. Copy right (2011) American Chemical Society).

Under visible-light illumination, electrons (e^-) of g-C_3N_4 are excited from the valence band (VB) to the conduction band (CB) , generating holes (h^+) in the VB. Generally, these charge carriers quickly recombine and only a section of electrons are injected into the Pt nanoparticles due to a Schottky barrier.[71,72] The injected electrons accumulate on the Pt nanoparticles and can effectively reduce H_2O (or H^+) to produce H_2, while holes accumulate at the valence band of g-C_3N_4 and can react with methanol as a sacrificial reagent. However, when g-C_3N_4 is immobilized on the surface of graphene sheets to form the layered composites, these photogenerated electrons on the CB of g-C_3N_4 could tend to transfer to graphene sheets due to their excellent electronic conductivity, restraining the electron-hole pair recombination.[68] The transferred electrons will accumulate on the Pt nanoparticles loaded on the graphene sheets via a percolation mechanism[73] and then participate in H_2 generation. The major reaction steps in this photocatalytic water-splitting mechanism under visible-light illumination are summarized by the following Eqs. (1)- (4).

$$\text{graphene/g-}C_3N_4 \xrightarrow{h\nu} \text{graphene } (e^-)/\text{g-}C_3N_4\ (h^+) \quad (1)$$

$$\text{graphene } (e^-) + \text{Pt} \rightarrow \text{graphene} + \text{Pt}\ (e^-) \quad (2)$$

$$\text{Pt}\ (e^-) + 2H^+ \rightarrow \text{Pt} + H_2 \quad (3)$$

$$\text{g-}C_3N_4\ (h^+) + CH_3OH + 6OH^- \rightarrow \text{g-}C_3N_4 + CO_2 + 5H_2O \quad (4)$$

And to date, a cross-linked g-C_3N_4/rGO (reduced graphene oxide) nanocomposites with tunable band structure was synthesized by Li et al, which demonstrated well-enhanced visible light photocatalytic activity.[74] Later, Wang et al noticed that a new class of ternary g-C_3N_4/Graphene/S nanoheterojunction was prepared by wrapping reduced graphene oxide and g-C_3N_4 sheets on crystals of cyclooctasulfur (α-S8) in bacterial inactivation under visible-light.[75] Except for the aforementioned achievement, a large numbers of attempts have been paid to explore novel materials coupling with g-C_3N_4 for broadening the applications of g-C_3N_4-based coupling heterojunction. In summary, these excellent g-C_3N_4 based non-metal nanoheterojunction are MWNTs (multi-walled carbon nanotubes)/g-C_3N_4,[76,77] polypyrrole/C_3N_4,[78] P/C_3N_4,[79] CN/CNS,[80] g-C_3N_4(from thiourea)/g-C_3N_4(from urea),[81] C_{60}/g-C_3N_4, as shown in Table 1.[82]

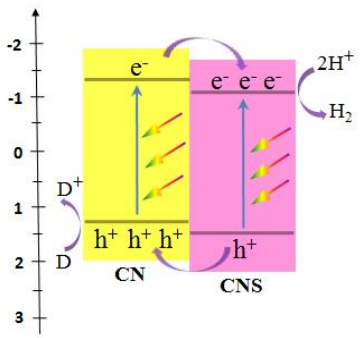

Fig. 2 Schematic illustration of organic heterojunction formed between CN and CNS. (CN refers to g-C_3N_4, CNS refers to sulfur-mediated CN, D=donor)

Significantly, Wang et al. obtained two types of host-guest CN/CNS heterojunctions (Fig. 2) with a facile band alignment by the surface-assisted polymerization: CNS–CN (CN serving as the host) and CN–CNS (CNS serving as the host).[80] CN/CNS isotype heterojunctions were obtained based on the band alignment between CN and CNS, owing to the slight difference in their electronic band structures. As an amazing result, these two types of CN/CNS heterojunctions mentioned above demonstrated conspicuous enhancement in the photocatalytic activity and stability for hydrogen evolution.

Inspired by Wang' work, the layered g-C_3N_4/g-C_3N_4 metal-free isotype heterojunction (Fig. 3a) was produced by treating the molecular composites precursors of urea and thiourea under the same thermal conditions. The molecular structure of this CN-T/CN-U heterojunction is illustrated in Fig. 3b. This isotype heterojunction was constructed on the basis that the g-C_3N_4 prepared from separate urea and thiourea has different band structure. Upon visible light irradiation, the photogenerated electrons transfer from g-C_3N_4 (thiourea) to g-C_3N_4 (urea) driven by the conduction band offset of 0.10 eV, whereas the photogenerated holes transfer from g-C_3N_4 (urea) to g-C_3N_4 (thiourea) driven by the valence band offset of 0.40 eV.[81] These two charge transfer processes are beneficial for overcoming the high dissociation barrier of the Frenkel exciton and stabilizing electrons and holes. The redistribution of electrons on one side of the heterojunction (CN-U) and holes on the opposite side (CN-T), could reduces the electron/hole pairs recombination as well as prolonged lifetime of charge carriers, resulting in exceptionally high photocatalytic capabiliy. These two successful works demonstrated that rational design and construction of isotype heterojunction could open up a new avenue for the development of new efficient visible-light photocatalysts.

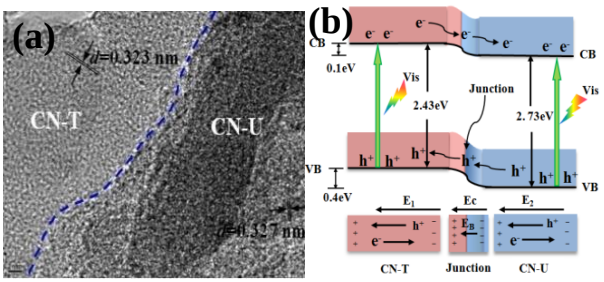

Fig. 3 (a) TEM images of CN-TU; (b) Schematic illustration of electron-hole separation and transport at the g-C_3N_4/g-C_3N_4 heterojunction interface and in both semiconductors: E_C is the contact electric field for the two components; E_B is the potential barrier in the interfacial depletion layer (E_B<E_C during the photocatalytic reaction); E_1 and E_2 are the internal electric fields induced by the redistribution of the spatial charges in CN-T and CN-U, respectively. CN-T refers to g-C_3N_4 from thiourea and CN-U refers to g-C_3N_4 from urea. (reprinted with permission from ref. 81. Copyright (2013) American Chemical Society).

Table 1 Photocatalytic properties of g-C_3N_4 based metal-free heterojunction composite photocatalysts

Composite photocatalyst	Mass or molar fraction of g-C_3N_4	Typical parameters of photocatalytic experiments	Photocatalytic activity	Reference photocatalyst; photocatalytic activity	Enhancement factor over the reference photocatalyst	Reference
Graphene / g-C_3N_4	Mass:99 %	Photocatalytic H_2 evolution under visible light; co-catalyst: Pt; sacrificial reagent: methanol	RH_2: 451μmol $h^{-1}g^{-1}$	g-C_3N_4: 147μmol $h^{-1}g^{-1}$ Graphene: no data	3.07 1.21	32
reduced graphene oxide (rGO) /g-C_3N_4	Mass:98.4% 97.5% 94.9% 80.4% Mass:98.4% 97.5% 94.9% 80.4%	Decomposing rhodamine B (RhB) under visible light Decomposing 4-nitrophenol under visible light	84%, in 75min 100%, in 75min 52%, in 75min 36%, in 75min No data, in150 min No data, in150 min No data, in150 min No data, in150 min	g-C_3N_4: 80% rGO: no data g-C_3N_4: no data rGO: no data	1.05 1.25 0.65 0.45 No data No data	74
multi-walled carbon nanotubes (MWNTs)/g-C_3N_4	Mass: 98%	Photocatalytic H_2 evolution under visible light; co-catalyst: Pt; sacrificial reagent: methanol	RH_2: 7.58μmol h^{-1}	g-C_3N_4: 2.03μmol h^{-1} MWNTs: no data	3.7 No data	76
multi-walled carbon nanotubes (CNT) /white C_3N_4	Mass:no data Mass:no data	Decomposing methyl orange (MO) under visible light Decomposing (RhB) under visible light	89.7% , in 3 h 85.4%, in 3 h	white C_3N_4: no data CNT: no data white C_3N_4: no data CNT: no data	No data No data No data No data	77
Polypyrrole (PPy) /g-C_3N_4	Mass:98.5% 99.5% 97.5% 96%	Photocatalytic H_2 evolution under visible light; co-catalyst: Pt; sacrificial reagent: no mention	RH_2:15.4μmol h^{-1} no data no data no data	g-C_3N_4: no data PPy: no data	No data No data	78
Red phosphor (r-P) /g-C_3N_4	Mass: 5% 30%	Photocatalytic H_2 evolution under visible light; co-catalyst: Pt; sacrificial reagent: Ascorbic acid	RH_2: 310μmol$h^{-1}g^{-1}$ 1000 μmol$h^{-1}g^{-1}$	g-C_3N_4: 340μmol$h^{-1}g^{-1}$ r-P:22μmol$h^{-1}g^{-1}$	0.91;14.09 2.94;45.45	79
Red phosphor (r-P) /g-C_3N_4	Mass: 30%	Photocatalytic CO_2 conversion into valuable hydrocarbon fuel (CH_4) in the presence of water vapor	295μmol$h^{-1}g^{-1}$	g-C_3N_4: 107μmol$h^{-1}g^{-1}$ r-P:145μmol$h^{-1}g^{-1}$	2.76 2.03	
RGO/ g-C_3N_4/ α-S_8 g-C_3N_4/RGO / α-S_8	Mass: 30%	Bacterial Inactivation (E.coliK-12) under Visible-Light	No data	g-C_3N_4: no data RGO: no data α-S_8: no data	No data No data No data	75
g-C_3N_4/C_{60}	Mass: 99.5% 99% 98%	Decomposing (RhB) under visible light	87%, in 60min 97%, in 60min 84%, in 60min	g-C_3N_4: 54% C_{60}: no data	1.61;1.80;1.56 No data	82
CNS/CN-2 CN/CNS-2	Mass: no data	Photocatalytic H_2 evolution under visible light; co-catalyst: Pt; sacrificial reagent: no mention	No data	CN: no data CNS: no data	11 2.3	80
g-C_3N_4/ g-C_3N_4	Mass: no data	Decomposing NO under visible light	47.6%, in 30min	g-C_3N_4:(T) 27.3% g-C_3N_4:(U) 31.7%	1.74 1.50	81
graphene/g-C_3N_4	Mass: no data	Conductivity and electrocatalytic performance on oxygen reduction reaction (ORR)	No data	g-C_3N_4:no data graphene:no data	No data No data	70

3.2 g-C_3N_4/single metal oxide (metal sulfide)

So far, various single metal oxides (metal sulfides) have been coupled with g-C_3N_4 to stability, appropriate band distribution for enhanced visible light photocatalysis.[83-87] Among abundant metal oxides, TiO_2 (Eg: 3.2ev) as a widely used photocatalyst, referentially acted as a candidate for constructing g-C_3N_4 based heterojunction. The work of Zhou et al., for example,

demonstrated that g-C_3N_4/TiO_2 nanotube array heterojunction was successfully achieved by a simple electrochemical method, showing highly effective visible-light performance with respect to bare g-C_3N_4 and TiO_2 nanotube.[45] Zhao el at obtained g-C_3N_4/TiO_2 hybrid photocatalyst by facile hydrolysis approach, accompanied with a remarkable enhancement of photocatalytic capability in degradation of phenol both under visible and UV light irradiation.[83] Sridharan et al successfully fabricated g-C_3N_4/TiO_2 composite with decent photocatalytic performance which was utilized in treatment of methylene blue (MB) and reduction of hazardous Cr(VI) ions.[84] Very recently, a direct Z-scheme g-C_3N_4/TiO_2 photocatalysts were successfully prepared via simple one-step calcinations with well photocatalytic response for formaldehyde decomposition in air, which was reported by Yu et al.[85]

WO_3 is another metal oxide that can be used to couple with g-C_3N_4. The band gap of WO_3 is between 2.6 and 2.8 eV.[88-90]. For instance, Zang et al obtained environmentally benign g-C_3N_4/WO_3 composite via facile mixing-heating procedure, which showed superb performance in methyl orange (MO) degradation.[88] A WO_3/g-C_3N_4 heterojunction (Fig. 4a, and 4b) was prepared by a calcination process accompanied with marvelous visible-light-activity by degradation of MB and 4-chlorophenol, documented by Huang et al.[89] Apparently, all of the WO_3/g-C_3N_4 photocatalysts demonstrated higher photocatalytic performance than the pristine WO_3, g-C_3N_4 as well as the mechanically blended WO_3 and g-C_3N_4 sample under visible light irradiation (Fig. 4c). Equally important, Katsumata et al have associated g-C_3N_4 with WO_3 by a physical mixing method to decontaminate the organic gas pollution acetaldehyde (CH_3CHO).[90]

The remarkably highly-increased performance of WO_3/g-C_3N_4 was mainly ascribed to the synergistic effects of the enhanced optical absorption in visible region, enlarged specific surface areas and the suitable band positions. A conceivable degradation mechanism was put forward as the Fig. 4d.

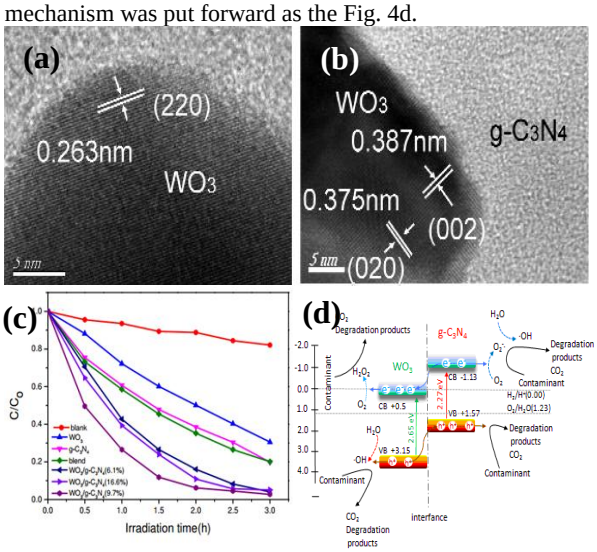

Fig. 4 (a,b) HRTEM images of WO_3/g-C_3N_4 (9.7%) composite; (c) Photocatalytic degradation efficiency of MB by g-C_3N_4, WO_3, blend and WO_3/g-C_3N_4 samples with different WO_3 contents under visible light; (d) Proposed mechanism for the photodegradation of contaminant on WO_3/g-C_3N_4 composite Reproduced from ref. 89 with permission from The Royal Society of Chemistry.

As can be seen in Fig. 4d, the top of the VB and the bottom of the CB of WO_3 were calculated to be 3.15eV and 0.5 eV, respectively.[89] In the case of g-C_3N_4, the top of the VB is 1.57 V and the bottom of the CB is -1.13V.[89] The band gaps of g-C_3N_4 and WO_3 were 2.70 eV and 2.65 eV, respectively. The pristine g-C_3N_4 and WO_3 are two semiconductors which can be both excited to produce photogenerated electron-hole pairs under visible light irradiation. Since the CB potential of (-1.13 eV) is lower than the CB edge of WO_3 (0.5eV), the excited-state electrons on g-C_3N_4 can directly inject into the CB of WO_3. Similarly, the VB position of WO_3 (+3.15 eV) is higher than the VB of g-C_3N_4 (+1.57 eV). The photogenerated holes on the VB of WO_3 can be directly injected to the VB of g-C_3N_4. The redistribution of electrons on one side of the junction (WO_3) and holes on the opposite side (g-C_3N_4) greatly reduces the electron-hole recombination, which is beneficial to promote the photocatalytic performance. As a result, the photocatalytic activity of WO_3/g-C_3N_4 composites was much higher than that of WO_3 and the pristine g-C_3N_4. Therefore, the enhanced photocatalytic activity was mainly associated to the heterojunction structure and the suitable band-edge positions of the two semiconductors, except for enhanced optical absorption in visible region and enlarged specific surface areas of WO_3/g-C_3N_4 nanojuctions,

Besides, Cadmium sulfide (CdS) is a fascinating semiconductor with relative low band gap of 2.4 eV, which makes it able to absorb solar light up to 520 nm or even longer.[86,87] Comparing the energy levels of C_3N_4 with CdS, it is fortunate to find that their well-matched band-structures are quite suitable to construct heterostructures that would bring an effective separation and transfer of photogenerated charges. To date, novel CdS/g-C_3N_4 organic–inorganic composites composed of two visible light responsive semiconductors have been fabricated via an "in situ" precipitation–deposition method by Fu et al, exhibiting outstanding visible light photocatalytic activity in 4-aminobenzoic acid removal.[42]

On account of multiple advantages of combining g-C_3N_4 with oxide (sulfide), a host of attempts have been devoted to exploit novel candidates for coupling with g-C_3N_4. They mainly include g-C_3N_4/Fe_2O_3,[89,91] g-C_3N_4/CeO_2[93] g-C_3N_4/MoO_3,[94] g-C_3N_4/Fe_3O_4[95] g-C_3N_4/$Ni(OH)_2$,[96] g-C_3N_4/Ag_2O,[97] g-C_3N_4/MoS_2[98] g-C_3N_4/ NiS,[99] g-C_3N_4/TaON,[30] g-C_3N_4/ZnO,[100,101] g-C_3N_4/In_2O_3,[102] g-C_3N_4/WO_3,[103] and SiO_2/g-C_3N_4.[104] These g-C_3N_4 based nanocomposites have become an important family of visible light photocatalysts for contaminants degradation and hydrogen production (Table 2).

Table 2 Photocatalytic properties of g-C_3N_4/single metal oxide (metal sulfide) nanocomposite photocatalysts

Composite photocatalyst	Mass fraction or molar of g-C_3N_4	Typical parameters of photocatalytic experiments	Photocatalytic activity	Reference photocatalyst; photocatalytic activity	Enhancement factor over the reference photocatalyst	Reference
TiO_2/g-C_3N_4	No data	Decomposing methyl orange (MO) under visible light	100% degradation in 30 min	g-C_3N_4:no data TiO_2: no data	No data 3	45
TiO_2/g-C_3N_4	300 °C 500°C	Decomposing Methylene Blue (MB) under visible light;	93%, 75% degradation in 120 min;	g-C_3N_4: no data TiO_2: no data	No data No data	84
TiO_2/g-C_3N_4	300 °C 500°C	Photocatalytic reduction of Cr(VI) under visible light	72% 45% in 100 min	g-C_3N_4: no data TiO_2: no data	No data No data	
TiO_2/g-C_3N_4	Mass: 20% Mass: 20%	Decomposing phenol under UV light Decomposing phenol under visible light	96.6% degradation in 60 min 67.7% degradation in 180 min	g-C_3N_4:79.5% TiO_2: 65.9% g-C_3N_4:43.8% TiO_2: no data	1.2 1.5 1.5 No data	83
TiO_2/g-C_3N_4	Mass: 16.7% 50% 66.7% 83.3%	Decomposing phenol under UV light	69.1%,in 60 min 82.7%, in 60 min 96.6% in 60 min 82.8%, in 60 min	g-C_3N_4:no data TiO_2: no data	No data No data	
TiO_2/g-C_3N_4 (Z-scheme)	Mass ratio: 100 % (urea:P25)	Decomposing formaldehyde under UV light	94%,in 60 min apparent rate constant k : 7.36 $\times 10^{-2}$min^{-1}	g-C_3N_4:no data TiO_2: no data g-C_3N_4:no data P25: 3.53$\times 10^{-2}$min^{-1}	No data No data No data 2.1	85
WO_3/g-C_3N_4	Mass ratio: no data	Decomposing (MO) under visible light	No data	g-C_3N_4:no data WO_3: no data	No data No data	88
WO_3/g-C_3N_4	Mass: 80% 60% 40% 20%	Decomposing acetaldehyde (CH_3CHO) under visible light	No data No data No data No data	g-C_3N_4:no data WO_3: no data	No data No data	90
WO_3/g-C_3N_4	Mass:90.3% Mass:90.3%	decomposing MB under visible light decomposing 4-chlorophenol (4-CP) under visible light	97% degradation in 2h 43% degradation in 6h	g-C_3N_4:81%,3h WO_3: 73%,3h g-C_3N_4:3%,6h WO_3: no data	1.2 1.3 14.3	89
a-Fe_2O_3/g-C_3N_4 precursors : [Bmim]$FeCl_4$ anhydrous FeCl	No data	Electrochemical properties	supercapacitive performance 167 Fg^{-1} 140 Fg^{-1}	g-C_3N_4: no data a-Fe_2O_3:72 Fg^{-1}	No data 2.3;1.9	91
Fe_2O_3/g-C_3N_4	Mass: 97.2% 95.1% 93.5% 92% 88.4%	Decomposing rhodamine B (RhB) under visible light	100%,in 120min 100%,in 160min 95.7%,in 180min 75.8%,in 180min 52.5%,in 180min	g-C_3N_4: 100%,180 min Fe_2O_3: no data	No data No data 0.96 0.76 0.53	9
ZnO/g-C_3N_4	Mass: 95.1% 91.6% 84.4 % 41.9%	Decomposing rhodamine B (RhB) under visible light	No data No data 97%, in 80 min No data	g-C_3N_4: no data ZnO: no data	No data No data	100
ZnO/g-C_3N_4	Mass: 84.4 %	Decomposing p-nitrophenol under visible light	No data	g-C_3N_4: 30%,5h ZnO: no data	No data No data	
ZnO/g-C_3N_4	Mass: 5.0% Mass: 5.0%	Decomposing (RhB) under visible light photoreduction of Cr^{6+} under visible light irradiation	97.4%, in 100 min 75.5%, in 100 min	g-C_3N_4: no data ZnO: no data g-C_3N_4: no data ZnO: no data	No data No data No data No data	101

CeO_2/g-C_3N_4	Mass: 87%	decomposing MB under visible light	95%, in120 min	g-C_3N_4: 75%,3h CeO_2: 28%,3h	1.3 3.4	93
	Mass: 94.1%, 87.0% 77.6%	decomposing 4-chlorophenol (4-CP) under visible light	30%, in5 h 45%, in5 h 37%, in5 h	g-C_3N_4: 2.3% CeO_2:15.1%	13.0;2.0 19.6;3.0 16.1;2.5	
MoO_3/g-C_3N_4	Mass: 7.0 %	decomposing MB under visible light	93%, in3 h	g-C_3N_4: no data MoO_3: no data	No data No data	94
Fe_3O_4/g-C_3N_4	Mass: 98 %	decomposing MO under visible light	No data	g-C_3N_4: no data Fe_3O_4: no data	No data No data	95
$Ni(OH)_2$/g-C_3N_4	Molar: 99.5 % 99.9 %	Photocatalytic H_2 evolution under visible light; co-catalyst: no; sacrificial reagent: triethanolamine	RH_2:7.6 mmol h^{-1} RH_2:3.3 mmol h^{-1}	g-C_3N_4: no data $Ni(OH)_2$: no data	No data No data	96
MoS_2/g-C_3N_4	Mass: 99.5 %	Photocatalytic H_2 evolution under visible light; co-catalyst: no; sacrificial reagent: lactic acid	RH_2:20.6mmolh^{-1}	g-C_3N_4: no data MoS_2: no data 0.5 wt % Pt/ g-C_3N_4: 4.8mmol h^{-1}	No data No data 4.3	98
CdS/g-C_3N_4	Mass: 70 %	Decomposing (MO) under visible light	92%, in20 min	g-C_3N_4:16%,in 25 min CdS: no data 0.3CdS–0.7TiO_2:19%, in 25 min	No data No data No data	42
	Mass: 70 %	Decomposing 4-aminobenzoic acid under visible light	73%, in60 min	0.7C_3N_4–0.3TiO_2:22%, in 25 min g-C_3N_4:3% CdS:38%	No data 2.7 41.6	
NiS/g-C_3N_4	Mass: 99.5 % 98.75 % 98 % 97.5 %	Photocatalytic H_2 evolution under visible light; co-catalyst: no; sacrificial reagent: triethanolamine	RH_2:9.2mmol h^{-1} RH_2:48.2mmol h^{-1} RH_2:32.1mmol h^{-1} RH_2:13.5mmol h^{-1}	g-C_3N_4:0.2mmol h^{-1} NiS: no data	46.0 241.0 160.5 67.5	99
TaON/g-C_3N_4	Mass: 60 %	Decomposing (RhB) under visible light	100%, in 50 min	g-C_3N_4:100%,in 80min TaON: 34%, in 80 min	No data No data	30
In_2O_3/g-C_3N_4	Mass: 90 %	CO_2 reduction into hydrocarbon fuels	CH_4 production yield：76.7 ppm	g-C_3N_4: no data In_2O_3: no data	3.0 4.0	102
WO_3/g-C_3N_4	Mass: 50 %	oxidation of acetaldehyde into CO_2	at least 600 ppm of acetaldehyde had been removed in 48h	g-C_3N_4: no data WO_3: no data	No data No data	103
SiO_2/g-C_3N_4	No data	Decomposing RhB under visible light	fully degraded in 60min	g-C_3N_4: no data SiO_2: no data	No data No data	104

3.3 g-C_3N_4/composite oxide

During the past few years, many groups have reported different types of g-C_3N_4/composite oxide heterojunction photocatalysts. These research studies greatly improve the efficiencies of the photocatalysts and promote their applications in the energy production and environmental remediation.[105,106]

Table 3 summarizes and compares the g-C_3N_4/composite oxide heterojunction photocatalysts. Among these photocatalytic systems, Bi_2WO_6/g-C_3N_4 has been the most widely investigated. Ge et al prepared g-C_3N_4/Bi_2WO_6 heterostructured photocatalysts via mixing and heating methods.[31] The g-C_3N_4/Bi_2WO_6 photocatalyst had a remarkably enhanced MO photodegradation activity than pure g-C_3N_4 and Bi_2WO_6 under visible light irradiation. This enhancement could be attributed to the enhanced visible-light utilization efficiency and accelerated transfer of photogenerated electron-hole pairs at the intimate interface of heterojunctions, which rationally can be ascribed to the well-aligned overlapping band-structures of g-C_3N_4 and Bi_2WO_6. Subsequently, Wang et al prepared Bi_2WO_6 hybridized with g-C_3N_4 by facile chemisorptions, which exhibited enhanced photocatalytic performance in MB degradation.[105] Tian et al hydrothermally synthesized a heterojunction by combining g-C_3N_4 with Bi_2WO_6 with enhanced visible light photocatalytic capbility.[106]

Li chose $SmVO_4$ (band gap 2.28eV) as a promising candidate for constructing g-C_3N_4 coupling heterojunction, and this g-C_3N_4/$SmVO_4$ composite photocatalyst exhibited high photocatalytic activity and stability for RhB decomposition under visible light irradiation.[107] Moreover, earth abundant cobalt phosphate (Co–Pi) has been demonstrated to work effectively as oxygen-evolving electrocatalyst[108-110] owing to its attractive characteristics such as the low cost and self-repairing behavior.[111,112] Recently, The Co–Pi species are presented as

nanoparticles and well-distributed on the g-C_3N_4 surface, and the Co–Pi/g-C_3N_4 composites exhibit stronger visible light absorption. The Co–Pi/g-C_3N_4 composite samples show significantly enhanced H_2 and O_2 evolution activities.[113]

It is well known that $ZnWO_4$ itself cannot be excited by visible light. On the contrary, C_3N_4 can absorb the visible light. Wang et al fabricated C_3N_4/$ZnWO_4$ coupling composite (Fig. 5a,b), i.e. the $ZnWO_4$, a semiconductor without visible photocatalytic performance was successfully photo-sensitized by g-C_3N_4.[114] These composites possessed eminent and commendably durable photocatalytic activity in removal of Rh-B, as well as enhanced photocurrent responses under visible light irradiation (Fig. 5c). More importantly, an new mechanism of $ZnWO_4$ sensitized by carbon nitride was presented in Fig. 5d.

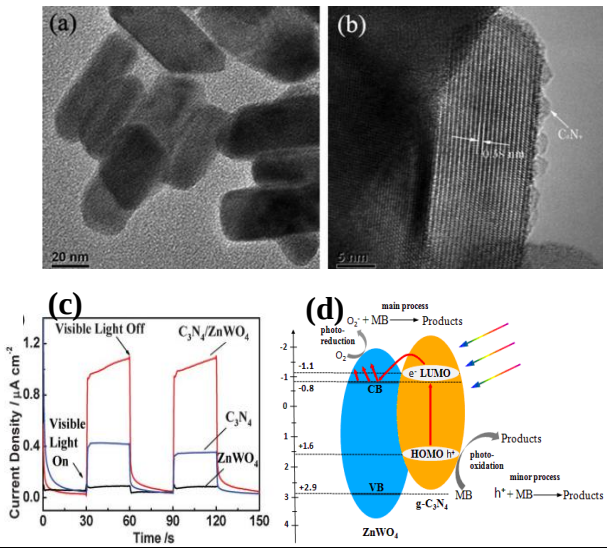

Fig. 5 HRTEM images of $ZnWO_4$ and C_3N_4/$ZnWO_4$ photocatalysts (a) $ZnWO_4$ (b) C_3N_4/$ZnWO_4$; (c) Photocurrents of $ZnWO_4$ and C_3N_4/$ZnWO_4$ electrodes with light on/off cycles under visible light irradiation (λ>420 nm) ([Na_2SO_4]=0.1M); (d) Schematic drawing of C_3N_4/$ZnWO_4$ photocatalyst under visible light. Reprinted with permission from ref. 114. Copyright (2012) The Royal Society of Chemistry.

Under visible light illumination, the excited-state electrons of the HOMO of the C_3N_4 would transport to the lower unoccupied molecular orbital (LUMO) of C_3N_4 (π–π* transition). Since the LUMO potential of C_3N_4 (-1.1 eV)[115] is lower than the CB edge of $ZnWO_4$ (-0.8 eV)[116], a chemical interaction occurs between them. Hence the excited-state electrons on C_3N_4 can directly inject into the CB of $ZnWO_4$. The electrons subsequently transfer to the photocatalyst surface to react with water and oxygen to generate hydroxyl and superoxide radicals.[114] These reactive radicals are able to oxidize the pollutants. As a result, the CN polymer sensitized $ZnWO_4$ photocatalyst exhibits enhanced visible light photocatalytic performance. To further broaden the application, many groups have gained achievements on development of newly g-C_3N_4 based heterojunctions with superior performance in photocatalysis, such as C_3N_4/$BiPO_4$,[117] g-C_3N_4/Ag_3PO_4,[118,119] g-C_3N_4/N-In_2TiO_5,[120] g-C_3N_4/$GdVO_4$,[121] g-C_3N_4/$NaTaO_3$,[122] g-C_3N_4/Rh-$SrTiO_3$,[123] g-C_3N_4/$Bi_5Nb_3O_{15}$,[124] and g-C_3N_4/Ag_3VO_4.[125]

Table 3 Photocatalytic properties of g-C_3N_4/composite oxide heterojunction photocatalysts

Composite photocatalyst	Mass or molar fraction of g-C_3N_4	Typical parameters of photocatalytic experiments	Photocatalytic activity	Reference photocatalyst; photocatalytic activity	Enhancement factor over the reference photocatalyst	Reference
$BiPO_4$/g-C_3N_4	Mass:4%	Decomposing methyl blue (MB) under UV light	90% degradation in 5 min	$BiPO_4$: no data P25(TiO_2):no data	2.5 4.5	117
	Mass:10%	Decomposing MB under visible light	apparent rate constant k : 0.31 h^{-1}	g-C_3N_4:k=0.06 h^{-1}	5	
Bi_2WO_6/g-C_3N_4	Mass:2%	Decomposing (MB) under simulated solar irradiation	apparent rate constant: k : 1.0291 h^{-1}	Bi_2WO_6; k:0.6060 h^{-1}	1.67	105
Bi_2WO_6/g-C_3N_4	Mass:50%	Decomposing methyl orange (MO) under visible light	93% degradation in 120 min	g-C_3N_4: 31% Bi_2WO_6: 0.6%	3 155	106
Bi_2WO_6/g-C_3N_4	Mass: 5% 10% 30% 50% 70% 90%	Decomposing (MO) under visible light	21.1%,3h 76.0%,3h 45.2%,3h 89.6%,3h 99.9%,3h 84.4%,3h	g-C_3N_4, :81.4%	0.26 0.46 0.56 1.10 1.23 1.03	31
Ag_3PO_4/g-C_3N_4	Mass:16.7%	Decomposing RhB under visible light	No data	g-C_3N_4, : no data Ag_3PO_4: no data	3.27 1.65	118
Ag_3PO_4/g-C_3N_4	Mass:25%	Decomposing (MO) under visible light	No data	g-C_3N_4 : no data Ag_3PO_4: no data	5 3.5	119
$ZnWO_4$/g-C_3N_4	Mass: 5%	Decomposing MB under UV light and visible light	No data No data	g-C_3N_4, : no data g-C_3N_4, : no data	1.8 No data	114

$GdVO_4$/g-C_3N_4	Mass: 90%	Decomposing (RhB) under visible light	apparent rate constant: k: 0.0434 min^{-1}	g-C_3N_4: no data N–TiO_2: no data $GdVO_4$: no data	3.1 6.3 36	121
$NaTaO_3$/g-C_3N_4	Mass: 5% 10%	Decomposing (RhB) under UV light and visible light	No data	g-C_3N_4: $NaTaO_3$: Degussa P25:	No data No data No data	122
$SrTiO_3$: Rh / g-C_3N_4	Mass: 30% 20% 10%	Photocatalytic H_2 evolution under visible light; co-catalyst: no; sacrificial reagent: not mentioned	RH_2: 81.0 $mmol^{-1}$ 223.3 92.6	g-C_3N_4;RH_2:10.7 $SrTiO_3$:Rh(0.3 mol%): 68.9	7.57, 1.2 20.9, 3.24 8.7, 1.3	123
$Bi_5Nb_3O_{15}$ / g-C_3N_4	Mass: 50% 70% 90% Mass:70%	Decomposing (MO) under visible light Decomposing 4-chlorophenol (4-CP) under visible light	86%, in 3h 94%, in 3h 93%, in 3h 100%, in 1h	g-C_3N_4: 80% $Bi_5Nb_3O_{15}$: 28% g-C_3N_4: 72% $Bi_5Nb_3O_{15}$: 38%	1.07; 3.1 1.2; 3.4 1.2; 3.3 1.4 2.6	124
$Co_3(PO_4)$/ g-C_3N_{42}	CP-20 (UV irradiation time: 20min)	Photocatalytic O_2 evolution under visible light; co-catalyst: no; sacrificial reagent:$AgNO_3$	No data, 3h	g-C_3N_4:1.28μmol	6.8	110
$Co_3(PO_4)_2$/ g-C_3N_4	CP-5 CP-10 CP-20 CP-30 CP-60	H_2 evolution under visible light	No data No data 19.48μmolh−1 No data No data	g-C_3N_4:2.03μmolh−1	No data No data 9.6 No data No data	
N-In_2TiO_5/ g-C_3N_4	No data	Decomposing (RhB) under visible light	degraded completely within 20 min	g-C_3N_4: no data N-In_2TiO_5:no data	No data No data	120
Ag_3VO_4/ g-C_3N_4	Mass: 10% 40% 50%	Decomposing basic fuchsin (BF) under visible light	60%, in 2.5h 95%, in 2.5h 88%, in 2.5h	g-C_3N_4: 15% Ag_3VO_4:30%	4.0; 2.0 6.3; 3.2 5.9; 2.9	125
Ag_3VO_4/ g-C_3N_4	Mass: 10%	malachite green (MG)	97%, in 1h	g-C_3N_4: no data Ag_3VO_4:no data	No data No data	
Ag_3VO_4/ g-C_3N_4	Mass: 10%	crystal violet (CV)	75%, in 2.5h	g-C_3N_4: no data Ag_3VO_4: no data	No data No data	
$SmVO_4$/ g-C_3N_4	Mass:50.3%	Decomposing (RhB) under visible light	2.07 h^{-1}	g-C_3N_4: no data $SmVO_4$: no data	2.4 6.3	104

3.4 g-C_3N_4/BiOX (AgX)

Recently, as halide, BiOX (X = Cl, Br, I) with advantages of layered structure and indirect-transition band-gap were reported as an efficient photocatalysts.[126-134] The layered structure can provide a large enough space to polarize the related atoms and orbitals, and then induce the presence of internal static electric fields perpendicular to the [Bi_2O_2] slabs and halogen anionic slabs in BiOX.[135-137] It is interesting to couple BiOX with g-C_3N_4 to form layered nanojunctions.

Among the BiOX photocatalysts, BiOBr with an appropriate band-gap (2.75 eV) exhibits high photocatalytic activity. Ye et al synthesized BiOBr-g-C_3N_4 inorganic–organic composite photocatalysts by a one-step chemical bath method at low temperature.[138] This heterojunction interacted by facets coupling contributes to the promoted photoinduced charges transfer between BiOBr and g-C_3N_4, and enhances the VLD photocatalytic activity for RhB degradation comparing with bare BiOBr and g-C_3N_4. Furthermore, Sun et al fabricated BiOBr-C_3N_4 heterojunction (Fig. 6a) by depositing BiOBr nanosheets onto the surface of C_3N_4 nanosheets at room temperature.[139] The heterojunction possess intimately contacted interfaces and well-aligned straddling band-structures, which are propitious to the effective separation and transfer of photogenerated charges, bringing an excellent performance. A schematic illustration of the band gap structures for the samples is shown in Fig. 6b.

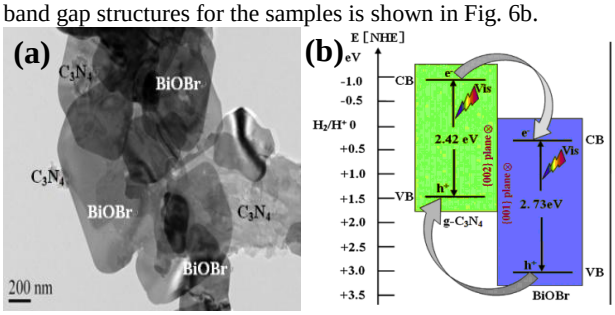

Fig. 6 TEM of the as-synthesized BiOBr/C_3N_4 nanojunctions (a) and Schematic illustration of the band-gap matching and the crystal-plane coupling of C_3N_4/BiOBr nanojunctions (b). Reproduced with permission from ref. 139, copyright 2014, Elsevier.

The band structures of the two components are well-matched and aligned with each other (Fig. 6b). Both C_3N_4 and BiOBr can be excited by visible light and then generate photo-induced electrons and holes. The relative CB and VB edge positions of C_3N_4 nanosheets and BiOBr nanosheets imply that the well-matched band energies and crystal planes can form heterojunctions at nanoscale level. The excited electrons in CB of C_3N_4 can transfer

to CB of BiOBr, and excited holes in VB of BiOBr can transfer to VB of C_3N_4, which results in efficient separation and transport of photo-induced electrons and holes. The 2D BiOBr/C_3N_4 layered nanojunctions could effectively strengthen the photocatalytic activity. This work demonstrated that novel 2D nanojunction, accompanied with high visible light activity can be constructed by combining two visible-light-active 2D semiconductors with well-coupled crystal planes and well-matched band structure, which could provide a new approach for promoting the activity of current photocatalysts.

BiOI is an attractive p-type semiconductor with the strong photoresponse in the visible light region due to its narrow band gap energy (1.78 eV) and could act as a potential sensitizer to sensitize wide band gap semiconductors. Until now, Jiang et al obtained novel p–n heterojunction photocatalyst constructed by porous graphite-like C_3N_4 and nanostructured BiOI.[140] In fact, the coupling of p- and n-type semiconductors is believed to be helpful because an internal electric field is built up between them. As a result, the coupling of n-type g-C_3N_4 with a p-type narrow band gap BiOI semiconductor is a good strategy to enhance the visible light absorption capability and the photocatalytic performance of g-C_3N_4 under visible light irradiation. Besides, Wang and his group successfully used BiOCl as an alternative to prepare BiOCl/C_3N_4 heterojunction photocatalysts via an ionic-liquid-assisted solvent-thermal route, and this nanocomposites demonstrated significantly enhanced visible light performance in degradation of MO due the formation of well-matched heterostructure.[141]

AgX based photocatalysts have attracted great attention as promising candidates for the development of highly efficient visible light photocatalysts. Some efforts were made to explore new-type g-C_3N_4 based heterojunction by coupling silver halide. Silver halide AgX (X = Br, I) is a photosensitive material extensively used in photography field.[142-144] Up to now, Xu et al successfully applied AgX (X = Br, I) developing novel visible-light-driven AgX/graphite-like C_3N_4(X=Br, I) hybrid materials and the photocatalytic activity dramatically improved, using methyl orange (MO) as a target pollutan.[145] The high photocatalytic activity of the hybrid materials could be ascribed to the strong coupling between g-C_3N_4 and AgX, which facilitated interfacial charge transfer and inhibited electron-hole recombination. Table 4 summarizes the photocatalytic properties of different g-C_3N_4/BiOX (AgX) composite photocatalysts.

Table 4 Photocatalytic properties of g-C_3N_4/BiOX (AgX) nanocomposite photocatalysts

Composite photocatalyst	Mass or molar fraction of g-C_3N_4	Typical parameters of photocatalytic experiments	Photocatalytic activity	Reference photocatalyst; photocatalytic activity	Enhancement factor over the reference photocatalyst	Reference
BiOBr /g-C_3N_4	Mass:50%	Decomposing rhodamine B (RhB) under visible light	95% degradation in 30 min	g-C_3N_4:15% BiOBr:35%	6.3 2.7	138
BiOBr /g-C_3N_4	Mass:50%	NO removal under visible light	32.7% degradation in 30 min	g-C_3N_4:22.9% BiOBr: 21.2%	1.4 1.5	139
BiOCl /g-C_3N_4	Molar: 50%	Decomposing methyl orange (MO) under visible light	95% degradation in 80 min	g-C_3N_4:11% BiOCl:58%	8.6 1.6	141
BiOI /g-C_3N_4	Mass:77.5%	Decomposing methyl blue (MB) under visible light	99% degradation in 3h	g-C_3N_4:64% BiOI: 51%	1.5 1.9	140
AgBr /g-C_3N_4	Molar:70%	Decomposing MO under visible light	91% degradation in 10h	g-C_3N_4: low AgBr:23%	No data 4	145
AgI /g-C_3N_4	Molar: 97.5% 95% 90% 70% 50%	Decomposing MO under visible light	28%, 3.5h 44%, 3.5h 79%, 3.5h 81%, 3.5h 62%, 3.5h	g-C_3N_4:no data AgI: no data	No data No data	
AgBr /g-C_3N_4	Molar: 70%	Decomposing 4-chlorophenol under visible light	30%, 6h	g-C_3N_4:6.1% AgBr: no data	4.9 No data	
AgI /g-C_3N_4	Molar: 70%	Decomposing 4-chlorophenol under visible light	53%, 6h	g-C_3N_4:6.1% AgI: no data	8.7 No data	

3.5 g-C_3N_4/noble metal

Semiconductor-metal junction is widely used to create a space-charge separation region (called the Schottky barrier). At the interface of the two components, electrons transfer from one component to the other to align the Fermi energy levels, preventing the charge recombination and enhancing photocatalytic performance. On the other hand, the surface plasmon renasance (SPR) endowed with noble matals could could increase the visibe light utilization and probably show special synegestic effectS with g-C_3N_4.[146-154] It is therefore feasible to couple noble metals with g-C_3N_4 in order to enhance the photocatalytic activity.[155-161] The work of Di et al., for example, preferentially demonstrated that the deposition-precipitation method was successfully applied to prepare Au(III) nanoparticles on the surface of a structured polymeric g-C_3N_4.[155] The as-synthesized nanoscopic Au–semiconductor heterojunctions effectively accelerate charges transfer on the intimate interface between g-C_3N_4 and Au nanoparticles, enabling high photocatalytic hydrogen production. In addition, given that gold nanoparticles (AuNPs) can serve as photocatalysts for the degradation of dyes under visible-light irradiation through the surface plasmon effect,[156] it is expected that AuNPs/g-C_3N_4 nanohybrids could show improved photocatalytic performance. Cheng et al proposed that Au nanoparticles (AuNPs) were successfully loaded on graphitic carbon nitride (g-C_3N_4), and the nanohybrids show superior photocatalytic activities for the

decomposition of methyl orange under visible-light irradiation due to the facilitated sepration of photogenerated electron-hole pairs, and the surface plasmon resonance excitation in AuNPs.[157]

It is well-documented that Ag, a famous noble metal, was regarded as a decent co-catalyst in constructing heterojunctions with g-C_3N_4 in photocatalytic utilizations.[158-159] Yang et al reported that an efficient visible-light plasmonic photocatalyst, Ag/g-C_3N_4 heterostructure, is facilely fabricated by a simple polymerization-photodeposition route.[158] Compared with individual g-C_3N_4, the photocatalytic activity of Ag/g-C_3N_4 was sharply enhanced toward the degradation of MO and p-nitrophenol, which may be ascribed to the enhanced visible-light utilization efficiency due to the SPR absorption of silver nanoparticles as well as fast generation, separation and transportation of the photogenerated carriers. Bai and his groups have developed novel core-shell Ag@g-C_3N_4 plasmonic nanocomposites by facile reflux treating method, exhibiting superb capability in photodegradation of MB and H_2 evolution.[159] Moreover, by embedding Pd nanoparticles on the g-C_3N_4, Pd/g-C_3N_4 metal-semiconductor heterojunction was constructed and demonstrated highly strengthened photocatalytic performance in bisphenol removal.[160] Meanwhile, note that Li et al have successfully obtained g-C_3N_4/noble metal by directly loading with Pt, Au and Pd NPs respectively via a conventional solution impregnation method.[161] The functional catalyst/support system can unambiguously act as a tandem catalyst to effectively trigger the water reduction reaction to form H_2 and activation of the as-formed H_2 for further reduction of 4-nitrophenol to 4-aminophenol.

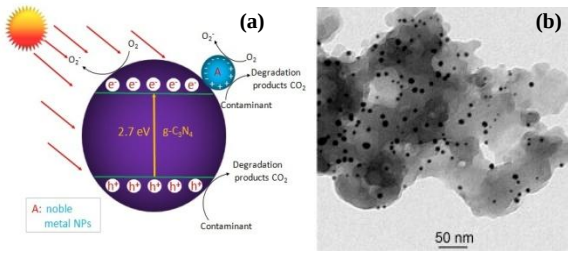

Fig. 7 (a) Schematic diagram illustrating the photocatalytic degradation of organic contaminants over noble metal NPs/g-C_3N_4 hybrid under visible-light irradiation; (b) TEM image of AuNP/g-C_3N_4 nanohybrids. Reprinted with permission from ref. 157. Copyright (2013) American Chemical Society.

g-C_3N_4 could function as an effective solid stabilizer for chaperoning various ultrafine noble metal NPs.[161] It is worthwhile to elucidate the function mechanisms of g-C_3N_4/noble metal nanohybrids with improved the photocatalytic performance. As an example of Au/g-C_3N_4 nanohybrids,[157] a schematic diagram on the phorocatalytic mechanism of Au/g-C_3N_4 is presented in Fig. 7a. Owing to surface plasmon resonance of noble metal$_4$, the as-prepared Au/g-C_3N_4 nanocomposites exhibit highly enhanced visible-light photocatalytic activity. On the one hand, the SPR effect of Au nanoparticle causes the intense local electromagnetic fields, which can speed the formation rate of holes and electrons within g-C_3N_4.[158-161] Additionally, the favorable Fermi level of noble metal facilitates the separation of electrons and holes, which in turn enhances the quantum efficiency of g-C_3N_4, due to the intimate combination of the noble metal/g-C_3N_4 nanohybrids (Fig. 7b).[162] Moreover, the transfer of electrons shifts the Fermi level to more negative potential, and thereby improving the reducibility of electrons in the Fermi level close to the CB of g-C_3N_4.[163] On the other hand, the efficient utilization of sunlight can be realized due to SPR absorption in the visible-light region as well as UV light response of the inter band transition of noble metal nanoparticles. Table 5 shows the photocatalytic properties of different g-C_3N_4/noble metal nanocomposite photocatalysts.

Table 5 Photocatalytic properties of g-C_3N_4/noble metal nanocomposite photocatalysts

Composite photocatalyst	Mass fraction or mass of g-C_3N_4	Typical parameters of photocatalytic experiments	Photocatalytic activity	Reference photocatalyst; photocatalytic activity	Enhancement factor over the reference photocatalyst	Reference
Au/g-C_3N_4	Mass:4.5%	Decomposing methyl orange (MO) under visible light	92.6% degradation in 150 min	g-C_3N_4: 28.7% Au: no data	3.2 No data	157
Au/g-C_3N_4 Pt-Au/g-C_3N_4 Pd-Au/g-C_3N_4 Ru-Au/g-C_3N_4 Ag-Au/g-C_3N_4	No data No data No data No data No data	Photocatalytic H_2 evolution under visible light; co-catalyst: no; sacrificial reagent: triethanolamine	RH_2: no data RH_2: no data RH_2: no data RH_2: no data RH_2: no data	Pt/g-C_3N_4; RH_2: no data	No data	15
m-CNR-Au(2nm) m-CNR-Pd(3nm) m-CNR-Pt(2 nm) m-CNR-Pt(2 nm)	No data No data No data No data	reduction of 4-nitrophenol to 4-aminophenol under visible light; Photocatalytic H_2 evolution Under a 300 W Xe lamp; co-catalyst: no; sacrificial reagent: triethanolamine	>96% in 5 min >85% H_2O convertion	No data No data	No data No data	161

Ag/g-C_3N_4	Ag : 0.1g Ag : 0.5g Ag : 1g Ag : 2g Ag : 5g	Decomposing MO under visible light	MO of 74% MO of 78% MO of 86% MO of 91% MO of 92%	g-C_3N_4:70%; P25 TiO_2:56%	1; 1.3 1.1; 1.4 1.2; 1.5 1.3; 1.6 1.3; 1.6	158
Ag/g-C_3N_4	Ag : 2g	Decomposing p-nitrophenol(PNP) under visible light	PNP of 98%	g-C_3N_4:83%; P25 TiO_2:<10%	1.2 >9.8	
Ag/g-C_3N_4	Mass:99.5%	Decomposing MO methyl blue (MB) phenol under visible light	No data No data	g-C_3N_4:no data g-C_3N_4:no data g-C_3N_4:no data	2.1 1.8 2.2	159
Ag/g-C_3N_4	Mass:90%	Photocatalytic H_2 evolution Under visible light; co-catalyst:no; sacrificial reagent: triethanolamine	No data	g-C_3N_4:no data	30	
Pd/g-C_3N_4	No data	Decomposing bisphenol A under solar light	93.9% Degradation in 180 min	Bulk g-C_3N_4: 6% P25 TiO_2: 6.7% g-C_3N_4: 52.1%	15.65 14.01 1.8	160

3.6 g-C_3N_4 based complex system

Although a number of g-C_3N_4-based two-component nanocomposites have been developed for enhanced visible light photocatalysis, there are still some shortages that needs to be further addressed. With this purpose, multicomponent complex heterojunction systems have been developed, in which two or more visible-light active components are integrated..[164-167] For example, novel Ag/AgBr/g-C_3N_4 ternary composite photocatalysts were successfully constructed via deposition-precipitation method, presenting dramatically improved photocatalytic performance for degradation of MO as well as good stability under visible light.[164]

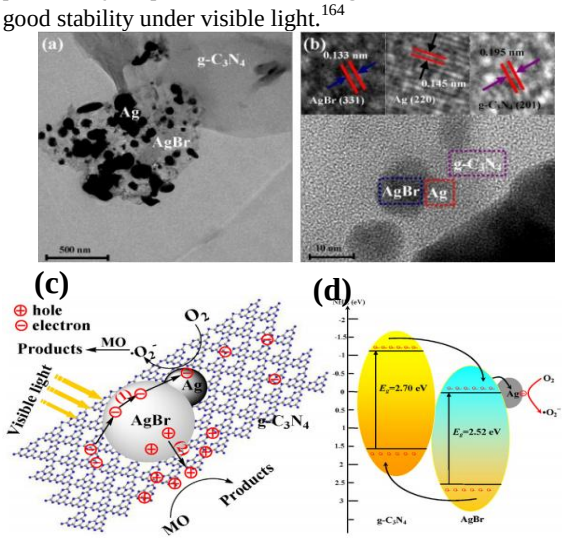

Fig. 8 (a) TEM image and (b) HRTEM image of 50% Ag/AgBr/g-C_3N_4; (c) Schematic diagram of electron-hole pairs separation and the possible reaction mechanism over Ag/AgBr/g-C_3N_4 photocatalyst under visible light irradiation. Reproduced with permission from ref. 164, copyright 2013, Elsevier.

The high photocatalytic activity and stability of Ag/AgBr/g-C_3N_4 mainly attributed to the synergetic effect of AgBr/g-C_3N_4 interface and metallic Ag (Fig. 8a and 8b). Namely, the matching energy band structure of AgBr/g-C_3N_4 and excellent electron trapping role of metallic Ag ensured the efficient separation of electron-hole pairs, i.e. metallic Ag quickly evacuated the electrons on the side of AgBr which guaranteed the stability of Ag/AgBr/g-C_3N_4, shown in Fig. 8c. Moreover, Chai et al. designed and prepared g-C_3N_4-Pt-TiO_2 three components nanocomposites via a facile chemical adsorption-calcination process, accompanied with remarkably enhanced performance for hydrogen production under visible light irradiation.[165] The cocatalyst Pt deposited on TiO_2 surfaces in the g-C_3N_4-TiO_2 heterojunction is beneficial for exerting the synergistic effect existing between TiO_2 and g-C_3N_4, which can strengthen the photogenerated carrier separation in space.

And inspiringly, a new-type Pt-TiO_2/g-C_3N_4-MnOx quaternary composites were also fabricated by a impregnation method with extraordinarily enhanced high H_2 production capacity, firstly reported by S. Obregón and G. Colón.[166] Such markedly increase in the photoactivity might be related the incorporation of Pt and g-C_3N_4-MnOx in the charge separation process, which is in favor of retarding the charge recombination and improving the photoactivity for H_2 production. A novel complex g-C_3N_4/CoO/graphene hybrid, with g-C_3N_4 embedded CoO particles covalently supported on a two-dimensional graphene sheet, is synthesized through a facile and scalable method by Jin and his co-workers.[167] Above all, these significant achievements can pave the way for constructing g-C_3N_4-based multi-component heterojunctions and it is highly possible to optimize the visible light absorption, the charge carriers separation and transfer by adequately tailoring the structure of the photocatalysts,.Recent progress on g-C_3N_4 based complex nanocomposites is summarized in Table 6.

Table 6 Photocatalytic properties of g-C_3N_4 based complex system

Composite photocatalyst	Mass or molar fraction of g-C_3N_4	Typical parameters of photocatalytic experiments	Photocatalytic activity	Reference photocatalyst; photocatalytic activity	Enhancement factor over the reference photocatalyst	Reference

Ag/AgBr/g-C_3N_4	Molar:5 0%	Decomposing methyl orange (MO) under visible light	95.3% degradation in 30 min	g-C_3N_4:2.5% Ag/AgBr:62.3%	38.1 1.5	164
Ag/AgBr/g-C_3N_4	Molar: 50%	Decomposing 2-chlorophenol under visible light	70.51% degradation in 4 h	No data	No data	
g-C_3N_4/Pt/TiO_2	Mass: 70%	Photocatalytic H_2 evolution under visible light; co-catalyst: no; sacrificial reagent: triethanolamine	RH_2: 0.178 mmol h^{-1}	Pt-loaded g-C_3N_4–TiO_2; RH_2:0.124 mmol h^{-1}	1.4	165
Pt-TiO_2/ g-C_3N_4-MnOx	No data	Decomposing phenol under UV light	96.4% degradation Time: no data	Pt- TiO_2:96.5% Pt-TiO_2/g-C_3N_4:96%	0.9 1.0	167
Pt-TiO_2/ g-C_3N_4-MnOx	No data	Photocatalytic H_2 Evolution under visible light; co-catalyst: no; sacrificial reagent: isopropanol	RH_2: 7.5 mmol $h^{-1}g^{-1}$	Pt- TiO_2; RH_2: 5.5 mmol $h^{-1}g^{-1}$ Pt- TiO_2/ g-C_3N_4; RH_2: 6.5 mmol $h^{-1}g^{-1}$	1.36 1.15	

4. Multifunctional applications

Semiconductor-mediated photocatalysis has attracted world-wide attention for its potential in environmental and energy-related applications.[45,117-125] Nevertheless, the rapid recombination rate of photogenerated electron-hole pairs within photocatalytic materials results in low efficiency, thus limiting its practical applications. Therefore, the retardation of recombination of charge carriers is the key for the enhancement of photocatalytic performance of semiconductor photocatalysts. g-C_3N_4-semiconductor hybrid materials as a new class of photocatalysts recently has attracted wide research interests.[138-141] In this regard, nanocomposites that combine g-C_3N_4 and other components could potentially provide desirable efficiency for separating electron-hole pairs. As documented above, the g-C_3N_4-based semiconductor photocatalysts have been widely used for the degradation of pollutants, photocatalytic hydrogen generation and photocatalytic conversion of carbon dioxide to methane fuel, etc. In this section the multiple applications of g-C_3N_4-based nanocomposite are briefly summarized.

4.1 Photocatalytic degradation of pollutants

In recent years, a large quantity of efforts has been devoted to solving the widespread pollution of effluents and gaseous pollutants from urban and agricultural industries. Various catalytic techniques have been applied in environmental conservation. Photocatalysis has been widely used in environmental applications such as air purification,[168-170] water disinfection,[171,172] hazardous waste remediation[173,174] and water decontamination.[175]

Graphene carbon nitrogen, as a ‘‘rising star’’ material has many exceptional properties, such as environmentally benign, stable physicochemical property, large specific surface area and low bad-gap, etc.[18-20] Hence, g-C_3N_4-based semiconductor photocatalysts have been extensively applied to photocatalytic degradation of environmental pollutants.[89,90] These composites possess high dye adsorption capacity, extended light absorption boundary, and accelerated charge transportation and separation properties.

For instance, a novel, multi-walled carbon nanotubes (CNT) modified white C_3N_4 composite (CNT/white C_3N_4) were fabricated by Xu et al.[77] The CNT/C_3N_4 nanocomposite was prepares by the hydrothermal method through electrostatically-driven self-assembly. The CNT/C_3N_4 composite shows significantly enhanced photocatalytic performance in MB dye removal. A possible photocatalytic mechanism of CNT/white C_3N_4 on the enhancement of visible light performance is proposed (Fig. 9a). Firstly, the electrons are motivated from the VB to the CB of C_3N_4 under visible light irradiation. Secondly, the photo-excited electrons are effectively collected by CNT, hindering the recombination process of the electron-hole pairs. Thirdly, the O_2 adsorbed on the surface of catalyst can be reduced to active species. The holes and the generated ·OH can react with the organic dye and generate degradation products. Furthermore, the photocatalytic stability of CNT/white C_3N_4 was investigated through the repeated MB degradation experiments, as shown in Fig. 9b. It is clear that the MB dye can be completely bleached after each photocatalytic run, and CNT/C_3N_4 is stable enough during the repeated experiments without significant loss of photocatalytic activity. Therefore, CNT/white C_3N_4 can be used as an effective photocatalyst for organic compounds degradation with good stability.

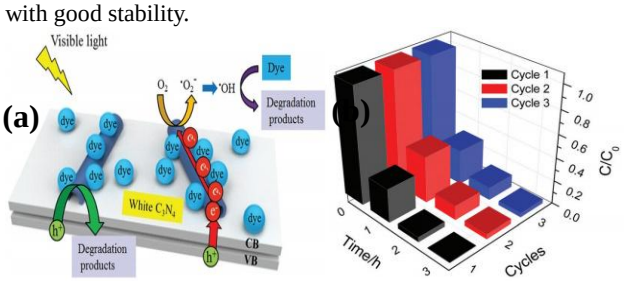

Fig. 9 (a) Proposed photocatalytic mechanism of the CNT/white C_3N_4; (b) Recycling in the repeated MB degradation experiments with CNT/white C_3N_4 under visible light irradiation. Reproduced with permission from ref. 77, Copyright (2013) The Royal Society of Chemistry..

Moreover, WO_3, a decent visible light catalyst was also selected to combine with g-C_3N_4.[89,90] Zang et al.[89] reported that the g-C_3N_4/WO_3 composite exhibited a significant enhancement of photocatalytic degradation of MO in water under visible light irradiation compared to the bare g-C_3N_4 and WO_3. As illustrated in Section 3 of g-C_3N_4/metal oxide (metal sulfide), In the g-C_3N_4/WO_3 composite, holes activated on the VB of the WO_3 would transfer to the VB of g-C_3N_4, while the electrons on CB of g-C_3N_4 may transfer to the CB of WO_3 under light irradiation due

to the well-matched energy band structure. Therefore, the photo-generated electrons and holes can be separated effectively in this way, and the recombination rate of the photo-generated electrons and holes would be hampered, which contributed to the superior photocatalytic reactivity. Moreover, this coupling heterojunction could also be used to remove the poisonous gaseous pollutant acetaldehyde gas (CH_3CHO), which is a typical volatile organic compound (VOC) and exerts adverse effects on the health of humans. By incorporating g-C_3N_4 with different contents of WO_3, Katsumata et al studied the photocatalytic performance of this composite in acetaldehyde gas removal.[90] As a result, they found that as the WO_3 content increases, the photodegradation effect became more conspicuous, and the optimum mass ratio of g-C_3N_4 to WO_3 for photocatalysis is two to eight.[90] What is more, Huang et al. further utilized this novel composite to treat another two organic pollutants of MB and 4-CP.[89]The highest degradation efficiency was achieved for the WO_3/g-C_3N_4 (9.7%) sample, which induced 97% degradation of MB within 2h and 43% degradation of 4-CP within 6h under visible light irradiation, while pristine g-C_3N_4 only induced 81% degradation of MB within 3h and 3% degradation of 4-CP within 6h.[89]

Apart from CNT/C_3N_4 and WO_3/g-C_3N_4 nanocomposites, composites of g-C_3N_4 and other semiconductor photocatalysts such as g-C_3N_4/TiO_2,[83,85] CeO_2/g-C_3N_4,[93] g-C_3N_4/CdS,[42] g-C_3N_4/TaON,[30] g-C_3N_4/Bi_2WO_6[105,106] BiOBr/g-C_3N_4,[138,139] BiOI/g-C_3N_4[140] and Pd/g-C_3N_4[160] have been reported as efficient photocatalysts for decomposition of pollutants in water. Among these coupling systems, TiO_2 as a famous UV light-driven and g-C_3N_4 as a robust visible-light-driven photocatalysts, are favourably selected to be coupled for enhanced photocatalysis. Zhao et al. evaluated both the UV and visible-light photocatalytic activity of g-C_3N_4/TiO_2 for degradation of phenol in water, and found that these composites exhibited excellent photocatalytic performance.[83] The pseudo-first-order kinetic constant of phenol degradation on g-C_3N_4/TiO_2 was 2.41 and 3.12 times higher that those on pristine g-C_3N_4 and TiO_2 respectively, which could be ascribed to the wide absorption wavelength range and effective photogenerated charge separation. Moreover, Fu and co-workers reported the g-C_3N_4 hybridized CdS composite as an efficient photocatalyst.[42] The optimum activity of 0.7C_3N_4-0.3CdS photocatalyst is almost 20.5 and 3.1 times higher than those of individual C_3N_4 and CdS for methyl orange degradation, and 41.6 and 2.7 fold higher for 4-aminobenzoic acid removal, respectively.[42] Moreover, its activity is also much higher than those of C_3N_4–TiO_2 and CdS–TiO_2 composites, as well as famous N-modified TiO_2. Of particular significance is that the present C_3N_4–CdS composites also demonstrate high stabilities under illumination, in contrast with CdS.[42] The improvement in both performance and stability should be assigned to the effective separation and transfer of photogenerated charges originating from the well-matched overlapping band-structures and closely contacted interfaces.

Recently, the g-C_3N_4-Bi_2WO_6 composite photocatalysts were studied by Tian and co-workers for the photocatalytic degrading MO under visible light irradiation.[106] Encouragingly, the resulting g-C_3N_4-Bi_2WO_6 heterojunctions own a strong absorption in the visible light region and have apparently enhanced photocatalytic performances. And this superior activity may be ascribed to the electronic interactions and charge equilibration between g-C_3N_4 and Bi_2WO_6, leading to the shift in the Fermi level and decreasing the conduction band potential of Bi_2WO_6. Simultaneously, the negative shift in the Fermi level of g-C_3N_4-Bi_2WO_6 and the high migration efficiency of photoinduced electrons can suppress the charge recombination effectively, resulting in the enhanced photocatalytic degradation of pollutants. Moreover, as bismuth subcarbonate ($(BiO)_2CO_3$) a novel photocatalyst, we achieved new g-C_3N_4/$(BiO)_2CO_3$ nanojunctions by a situ strategy depositing $(BiO)_2CO_3$ nanoflakes onto the surface of g-C_3N_4 nanosheets through efficiently capture atmospheric CO_2 (crude material of $(BiO)_2CO_3$) method at room temperature.[176] These nanojunctioned photocatalysts showed excellent visible-light capability by degrading RhB and phenol, accompanied by well-stability.

Hitherto, arrays of successful efforts of g-C_3N_4-based heterojunctions have also been paid to degrading NOx, which have been regarded as a worldwide gaseous pollutant. Our groups have investigated the photocatalytic capability of novel 2D BiOBr/C_3N_4 nanojunctions in NOx removal. [139] The NO removal ratios of BiOBr/C_3N_4 can be achieved to 32.7%, which is much higher than that of the pristine BiOBr (21.2%) and C_3N_4 (21.2%). The enhancement of photocatalytic performance of BiOBr/C_3N_4 could be ascribed to the synergistic effect of well-coupled crystal planes and band structure. To further boast the photocatalytic activities, we constructed the g-C_3N_4/g-C_3N_4 metal-free isotype heterojunction by a facile situ method.[81] The CN-TU dramatically exhibited an improved NO removal ratio of 47.6%, compared to host substrates of CN-U and CN-T. Besides, this metal-free isotype heterojunction demonstrated well stability as well. The strengthened photocatalytic performance of g-C_3N_4/g-C_3N_4 isotype heterojunction can be directly ascribed to the efficiently accelerated charge separation across the heterojunction interface as well as prolonged lifetime of charge carriers.

4.2 Photocatalytic hydrogen generation

Hydrogen energy is regarded as an ultimate clean fuel in the near future because of its high-energy capacity, environmental benignancy, and recycling utilization.[96,177,178] Photocatalytic splitting water into hydrogen and oxygen using semiconductor photocatalysts has been regarded as an attractive and promising approach to produce hydrogen energy. A flock of semiconductor photocatalysts have been reported to catalyze the evolution of hydrogen from water. However, the practical applications of this strategy are limited on account of the prompt recombination of photogenerated electron-hole pairs within photocatalysts. Considering the visible-light-driven property and high specific surface area, g-C_3N_4 can be regarded as an efficient photocatalyst for enhancing the visible light utilization and accelerating the photo-induced charge transfer hampering the backward reaction, which will highly promote the photocatalytic H_2-production activity.[179,180]

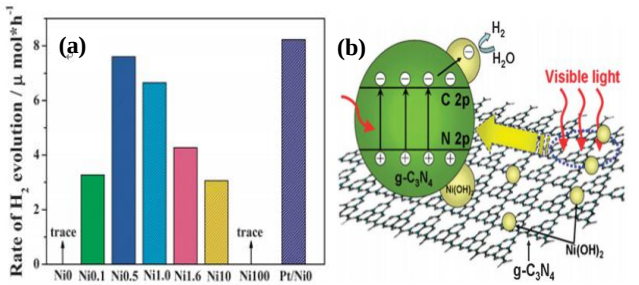

Fig. 10 (a) Comparison of the photocatalytic activity of the Ni0, Ni0.1, Ni0.5, Ni1.0, Ni1.6, Ni10, Ni100 and Pt-deposited g-C_3N_4 samples for the photocatalytic H_2 production from triethanolamine aqueous solution; (b) Schematic illustration for the charge transfer and separation in the $Ni(OH)_2$-modified g-C_3N_4 system under visible light irradiation. Reprinted with permission from ref. 96. Copyright (2013) The Royal Society of Chemistry.

$Ni(OH)_2$/g-C_3N_4 composites loaded with different contents of $Ni(OH)_2$, Yu and co-workers[96] studied their water splitting performance in triethanolamine aqueous solutions. The results demonstrated that $Ni(OH)_2$ was an efficient co-catalyst for g-C_3N_4 photocatalytic producing H_2. The optimal $Ni(OH)_2$ loaded on g-C_3N_4 was found to be 0.5 mol%, giving a H_2-production rate of 7.6 mmol h^{-1} with quantum efficiency (QE) of 1.1% at 420 nm, depicted in Fig.10a. The fact that the potential of Ni^{2+}/Ni is lower than that of the CB of g-C_3N_4 and more negative than that of H^+/H_2 favors the electron transfer from CB of g-C_3N_4 to $Ni(OH)_2$ and then reduce H^+ to H_2 with decent performance (Fig.10(b)). This work proved that $Ni(OH)_2$ was a very promising co-catalyst to combine with g-C_3N_4 for visible-light photocatalytic hydrogen production. Very recently, Hong et al [99] systematically studied the efficiency of H_2 evolution for the NiS/g-C_3N_4 composite constructed by a simple hydrothermal method. This photocatalyst showed efficient hydrogen evolution (48.2mmol h^{-1}) under visible light when using triethanolamine as a sacrificial reagent. The optimal ratios was 1.1 wt % of NiS loaded on g-C_3N_4 and the rates of H_2 production can be enhanced by about 250 times compared with the native C_3N_4. The highest apparent quantum efficiency was recorded at 1.9 % induced by 440 nm light irradiation. In order to further explore the possible application of g-C_3N_4/single metal oxide (metal sulfide) composites in hydrogen production, Hou and co-workers[98] constructed MoS_2/g-C_3N_4 nanojunctions and found that visible-light performance of H_2 production of mpg-CN is significantly improved compared with bare MoS_2 and g-C_3N_4. Inspiringly, the 0.5 wt % MoS_2/mpg-CN performed better than 0.5 wt % Pt/mpg-CN under identical reaction conditions. The geometric similarity (layered morphology) of MoS_2 and g-CN (Fig.11), accompanied with the mesoporous architectures of mpg-CN facilitate to forming intimate planar MoS_2/mpg-CN interface, which can significantly promote the photoactivity of MoS_2/ g-C_3N_4. They also discovered that other layered transition metal dichalcogenides (such as WS_2) are also efficient promoters for hydrogen production combined with g-C_3N_4. Herein they have presented not only an example of a catalyst made of abundant C, N, Mo and S elements for efficient H_2 photosynthesis, but also a conceptual advance to rationally design and fabricate a thin, effective interfacial 2D junctions between co-catalysts and semiconductors that have similar layered geometric architectures.

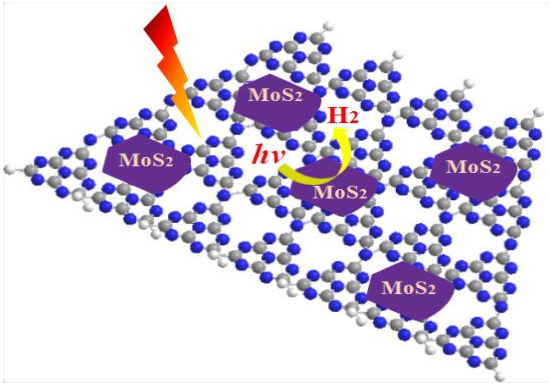

Fig. 11 Schematic illustration of the idealized structural model of the resultant MoS_2/g-CN layered junctions.

Apart from the g-C_3N_4/single metal oxide (sulfide) composites, researches have coupled C_3N_4 with other decent photocatalysts to further strengthen the H_2 generation efficiency. [155,123,165], Take noble metals as an example, Di al. reported that gold (Au) nanoparticles were successfully deposited on the surface of g-C_3N_4 by deposition–precipitation method.[155] The as-synthesized nanoscopic Au-semiconductor heterojunctions effectively accelerated the transfer of charges between g-C_3N_4 and Au, which can enable Au-g-C_3N_4 with excellent visible-light activity for hydrogen production. Besides, surface modifying Au/g-C_3N_4 with a second metal Pt (low over-potential for water reduction) further improved the activity of the photocatalytic system. This can be explained by simultaneous optimization of electron transfer induced by the gold and chemical reactivity afforded by the secondary metal Pt. Moreover, Kang and his groups systematically studied g-C_3N_4-$SrTiO_3$:Rh photocatalyst for improved H_2 evolution under visible light irradiation.[123] A high hydrogen evolution rate of 223.3 mmol h^{-1} was achieved by using 0.1 g of as-prepared photocatalyst powder comprised of 20 wt.% g-C_3N_4 and 80% $SrTiO_3$:Rh (0.3 mol%), measured in aqueous methanol solution. A mechanism for the electron-hole separation of the g-C_3N_4-$SrTiO_3$:Rh composite under visible light irradiation was proposed. The Rh ions doped into the $SrTiO_3$ lattice structure formed a donor level from the VB to CB, which eased the transfer of the photo-induced holes form the $SrTiO_3$:Rh surface to the g-C_3N_4 surface and the photo-induced electrons from the g-C_3N_4 surface to the $SrTiO_3$:Rh surface, thereby preventing the recombination of electron-hole pairs. Also, Chai et al. investigated a ternary nanocomposite g-C_3N_4–Pt-TiO_2 in photocatalytic hydrogen evolution.[165] The visible-light-induced photocatalytic hydrogen evolution rate can be remarkably strengthened by coupling TiO_2 with g-C_3N_4, and the g-C_3N_4–(Pt-TiO_2) composite with a mass ratio of 70: 30 shows the maximum photocatalytic H_2 production rate (178 mmol h^{-1}), as well as excellent photostability. Moreover, the cocatalyst Pt deposited on TiO_2 surfaces is beneficial for exerting the synergistic effect existing between TiO_2 and g-C_3N_4. Thus, the photogenerated electrons of g-C_3N_4 can directionally migrate to Pt-TiO_2 due to the close interfacial connections and the synergistic effect existing between Pt-TiO_2 and g-C_3N_4. The photogenerated electrons and holes can efficiently separated in space, beneficial for retarding the charge recombination and improving the photoactivity. This study not only shows that g-C_3N_4 as an

effective sensitizer of TiO_2 can be widely used to improve photocatalytic H_2 production, but also afforded various methods for developing novel, steady and visible-light-responsive photocatalysts.

Also, graphene, a two-dimensional macromolecular sheet of carbon atoms with a honeycomb structure, extremely high specific surface area and thermal conductivity, showed a good photocatalytic performance for hydrogen or oxygen production.[181] After introduction of graphene sheets, g-C_3N_4 is immobilized to form a layered composites，which will largely increase the BET and catalytic performance.[32] In this system, graphene sheets act as conductive channels efficiently separating the photogenerated charge carriers as well as enhancing the visible-light capability of H_2-production. The optimal graphene content was found to be 1.0 wt %, and the corresponding H_2-production rate was 451 μmol $h^{-1}g^{-1}$, which exceeded that of pure g-C_3N_4 more than 3.07 times. The potential mechanism was illustrated in Scheme 1. Normally, when g-C_3N_4 is immobilized on the surface of graphene sheets to form the layered composites, these photogenerated electrons on the CB of g-C_3N_4 tend to transfer to graphene sheets due to their excellent electronic conductivity, favoring the hole-electron separation. Meanwhile, Sui et al. reported that they have successfully loaded highly-dispersed conductive polymer polypyrrole (PPy) nanoparticles on the surface of g-C_3N_4.[76] Surprisingly, they found that the H_2 evolution rate of g-C_3N_4 loades with 1.5 wt% PPy can increase up to 50 times compared with that of pristine g-C_3N_4, and the reaction proceeded in a pure water system excluding the need of sacrificial agents. We believe that these work can provide an effective route for developing efficient photocatalysts for photocatalytic hydrogen evolution from pure water systems.

4.3 other applications

Solar fuels have been considered as one of the most important renewable clean energy resources and photocatalytic converting CO_2 into valuable hydrocarbon fuel (CH_4) is known as a challenging but promising application for sustainable energy resources.[76,182-186] In g-C_3N_4 based composites, Yuan et al. significantly obtained red phosphor/g-C_3N_4 heterojunction with enhanced photocatalytic activities for solar fuels production.[76] The introduction of g-C_3N_4 onto Red phosphor surface led to considerable improvement of the photocatalytic activity for CO_2 conversion into CH_4 in the presence of water vapor. The enhancement could be attributed to the effective separation of photogenerated electrons and holes across the red phosphor/g-C_3N_4 heterojunction. Owing to the advantages of non-toxicity, low cost and abundance in nature, this active heterostructural red phosphor/g-C_3N_4 would have great potential for efficient solar fuels production. Very recently, In_2O_3/g-C_3N_4 hybrid photocatalysts were fabricated by Cao and his group, and the resulting In_2O_3–g-C_3N_4 hybrid structures exhibited considerable photocatalytic activities for CO_2 reduction.[102] After 4-h irradiation, the optimal In_2O_3/g-C_3N_4 (10 wt% In_2O_3) exhibited a CH_4 production yield of 76.7 ppm (over 20 mg samples) without any cocatalyst, which is more than three times higher than that of individual g-C_3N_4 and more than four times higher than that of pure In_2O_3. The enhanced activities were attributed to the enhanced interfacial transfer of photogenerated electrons and holes between g-C_3N_4 and In_2O_3, leading to effective charge separation on both parts.

Moveover, g-C_3N_4 based composites also were considered as a promising candidate in photocatalytic disinfection.[75] A novel class of metal-free ternary heterojunction photocatalysts was prepared by wrapping reduced graphene oxide and g-C_3N_4 sheets on crystals of cyclooctasulfur (α-S8), reported by Wang et al.[75] Two distinctive structures were fabricated by wrapping reduced graphene oxide (RGO) and CN sheets in different orders. The first was RGO sheets sandwiched in heterojunction of CN sheets and α-S_8 (i.e.,CNRGOS8), while the second structure was the other way around (i.e., RGOCNS_8).And fascinatingly, both structures exhibited outstanding antibacterial activity in aerobic or anaerobic conditions irradiated with visible light (Fig. 12), which chosed colibacillus as a representative microorganism to evaluate the photocatalytic water disinfection performances. This work not only provided new inroads into exploration and understanding the photocatalytic bacterial inactivation mechanisms, but also afforded to developing suitable protocols for solar-driven photocatalytic water disinfection under different conditions.

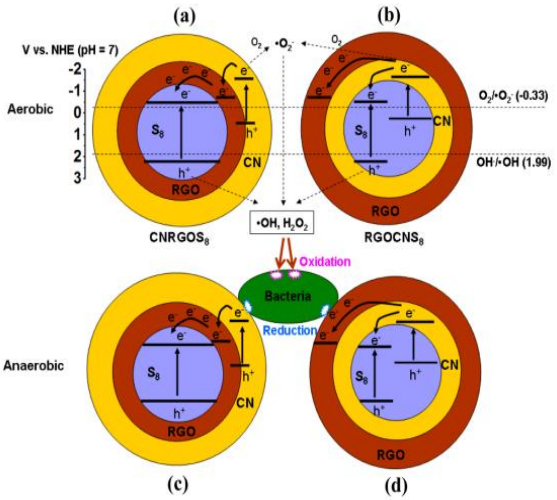

Fig. 12 Schematic illustration of the VLD photocatalytic bacterial inactivation mechanisms of (a) CNRGOS_8 and (b) RGOCNS_8 in aerobic condition, and (c) CNRGOS_8 and (d) RGOCNS_8 in anaerobic condition. (CNRGOS8 was RGO sheets sandwiched in heterojunction of CN sheets and α-S8, while RGOCNS8 was the other way around (i.e.,).Reprinted with permission from ref. 75. Copyright (2013) American Chemical Society.

In addition, g-C_3N_4-based heterojuctions are also utilized in performing as supercapacitors. Xu et al. mentioned that the g-C_3N_4/a-Fe_2O_3 hollow microspheres have been successfully prepared in the presence of metal ion-containing reactable ionic liquid under the solvothermal condition.[91] The capacitance of the g-C_3N_4/a-Fe_2O_3 composites as electrode materials was tested by cyclic voltammetry and chronopotentiometry measurements, demonstrating that the g-C_3N_4/a-Fe_2O_3 composites were capable of delivering a largest specific capacitance and highest coulombic efficiency. It can be assumed that the enhanced specific capacitance of the g-C_3N_4/a-Fe_2O_3 hollow microspheres could be attributed to hollow spheres-like structures, high BET surface area, incorporation of g-C_3N_4, and low electronic resistance. Thus, the g-C_3N_4/a-Fe_2O_3 hollow microspheres are promising candidate

for high-performance supercapacitors.

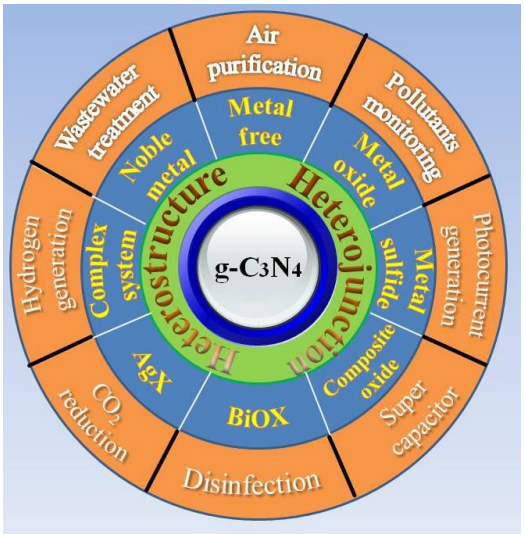

Fig. 13 Schematic illustration of the g-C_3N_4 based heterojunction/heterostructure and their multifunctional applications.

We have made a summary of the design strategy, categories and their multifunctional applications of g-C_3N_4 based nanocomposites as illustrated in Fig. 13.

5. Conclusion and perspectives

In summary, various types of g-C_3N_4-based nanocomposites system have been designed and constructed. The incorporation of g-C_3N_4 into these nanocomposites can impart them with unique properties and induce enhanced performance, such as high adsorption capacity, extended light absorption range, and accelerated charge separation and transportation, which strengthen the overall photocatalytic performance. A wide range of heterostructures, including metal-free, metal/semiconductor, semiconductor/semiconductor, molecule/semiconductor, and multi-component heterostructures, have been explored for the improved photocatalysis by increasing the light absorption, improving the charge separation and transportation, enhancing the catalytic activity and prolonging the charge carriers lifetime. These nanocomposites photocatalysts have been widely used for photocatalytic degradation of pollutants, photocatalytic hydrogen generation, carbon dioxide storage and disinfection. The present review depicts the fabrication, microstructure and photocatalytic performance, as well as the photocatalytic mechanisms when g-C_3N_4 is coupled with an array of materials such as metal-free, single metal oxide (metal sulfide), composite oxide, halide, noble metal, *etc*. It is anticipated that the g-C_3N_4-based nanocomposites will receive ever increasing research interest in the future.

Although considerable progress has been achieved, the studies in this field are still at the primary stage and further systematic investigations are needed. Rational design of complex heterostructures that could simultaneously facilitate efficient optical absorption, carrier generation, separation, transportation and utilizations is central for a new generation of highly efficient and robust photocatalysts. Significant challenges remain in the synthesis of such complex nanostructures with well designed architectures and optimized charge cascading processes.

First, a fundamental understanding of the charge transport process in the multi-heterostructure photocatalysts is critical for the optimization of the charge cascading process to maximize the utilization of photogenerated charge carriers for desirable redox chemistry. While it is relatively straightforward to understand electron/hole separation and transportation in a two component heterostructure, the understanding and control of charge transport in multi-component heterostructure become increasingly more complex, particularly on the nanometer scale. The interface properties of the photocatalysts determine the eventual efficiency of the photocatalytic system. To understand the charge generation, separation and transportation across these nanoscale interfaces is critical. Current investigations mainly focus on an overall apparent efficiency of the entire photocatalytic system. The detailed mechanism studies of the charge transfer process in photocatalysts integrating three or more components are scarce and will be necessary to further advance the field.

Secondly, the stability of g-C_3N_4-based nanocomposites is less addressed and will be one main challenge for photocatalyst development. A photocatalyst with very high efficiency is still useless if the lifetime of the catalyst is too short. For majority of systems, chemical corrosion and/or photodegradation of photocatalysts are difficult to avoid. The promoted photocatalyst stability has only been achieved in a few examples to date, which usually however, requires highly complicated synthetic processes. To develop a stable photocatalytic system with high efficiency at low-cost will be the central task to realize a practically viable photocatalyst for potential practical applications.

Thirdly, the mechanisms of photocatalytic enhancement by the g-C_3N_4-based semiconductor composite systems are partly unclear. And the explanation of photocatalytic activity by the g-C_3N_4 content in the composites is still controversial. Therefore, more studies are required to promote the general understanding of the enhancement mechanism of g-C_3N_4 based nanocomposites, especially employing advanced in situ techniques. Also, it is necessary to develop a uniform method to assess the photocatalytic performance as the current evaluation methods are diverse. A photocatalyst working better in water treatment may show poor performace in air purification.

Finally, the rapid development of material science and nanotechnology in the past few years has resulted in the creation of various advanced photocatalytic materials. Interesting properties may be explored by combining novel photocatalysts with g-C_3N_4. With a better understanding of the fundamental photocatalysis mechanism, assisted by the rapid development of advanced new nanomaterials, the bottleneck of environmental and energy-related global issues could be overcome in the near future. Overall, it is certain that there will be numerous exciting opportunities on g-C_3N_4 based nanocomposites, which require the combined efforts of scientists all over the world.

Acknowledgements

This research is financially supported by the National Natural Science Foundation of China (51478070, 51108487), the Natural Science Foundation Project of CQ CSTC (cstc2013jcyjA20018), the Science and Technology Project from Chongqing Education Commission (KJ1400617, KJ130725), and the Innovative Research Team Development Program in University of Chongqing (KJTD201314).

Notes and references

1 C.C. Chen, W.H. Ma, J.C. Zhao, *Chem. Soc. Rev.*, 2010, **39**, 206–4219.
2 G. Liu, L.Z. Wang, H.G. Yang, H.M. Cheng and G.Q. Lu, *J. Mater. Chem.*, 2010, **20**, 831–843.
3 D.Q. Zhang, G.S. Li and J.C. Yu, *J. Mater. Chem.*, 2010, **20**, 4529–4536.
4 M.D. Hernandez-Alonso, F. Fresno, S. Suarez and J.M. Coronado, *Energy Environ. Sci.*, 2009, **2**, 1231–1257.
5 H. Tong, S. Ouyang, Y. Bi, N. Umezawa, M. Oshikiri and J. Ye, *Adv. Mater.*, 2012, **24**, 229-251
6 M.L. de Souza and P. Corio, *Appl. Catal. B: Environ.*, 2013, **136–137,** 325–333.
7 M. Radoiˇ ci´ c, Z.ˇSaponji´ c, I.A. Jankovi´ c, G.´ Ciri´ c-Marjanovi´c, S.P. Ahrenkiel and M.I. Comor, *Appl. Catal. B: Environ.*, 2013, **136**–**137**, 133–139.
8 M.B. Radoiˇci´c, I.A. Jankovi´c, V.N. Despotovi´c, D.V.ˇSoji´ c, T.D. Savi´c, Z.V.ˇSaponji´ c, B.F. Abramovi´c, M.I.ˇComor, *Appl. Catal. B: Environ.*, 2013, **138/139** ,122–127.
9 J.X. Wang, P.X. Wang, Y.T. Cao, J. Chen, W.J. Li, Y. Shao, Y. and D.Z. Li, *Appl. Catal. B: Environ.*, 2013, **136**–**137**, 94–102.
10 T.T. Li, Y.M. He, H.J. Lin, J. Cai, L.Z. Dong, X.X. Wang, M.F. Luo, L.H. Zhao, X.D. Yi and W.Z. Weng, *Appl. Catal. B: Environ.*, 2013, **138**–**139**, 95–103.
11 W.D. Shi, J.Q. Shi, S. Yu and P. Liu, *Appl. Catal. B: Environ.*, 2013 ,**138**–**139**, 184–190.
12 D.G. Wang, H.F. Jiang, X. Zong, Q. Xu, Y. Ma, G.L. Li and C. Li, *Chem.-Eur. J.*, 2011, **17**, 1275–1282.
13 Y.N. Guo, L. Chen, X. Yang, F.Y. Ma, S.Q. Zhang, Y.X. Yang, Y.H. Guo and X. Yuan, *RSC Adv.*, 2012, **24**, 656–4663.
14 D.Q. He, L.L. Wang, D.D. Xu, J.L. Zhai and D.J. Wang T.F. Xie, *ACS Appl. Mater. Interfaces.*, 2011, **3**, 3167–3171.
15 K.Maeda, *Phys. Chem. Chem. Phys.*, 2013, **15**, 10537–10548.
16 B. Siritanaratkul, K. Maeda, T. Hisatomi and K. Domen, *ChemSusChem*, 2011, **4**, 7–78.
17 J.G. Hou, Z. Wang, W.B. Kan, S.Q. Jiao, H.M. Zhu and R.V. Kumar, *J. Mater. Chem.*, 2012, **22**, 7291–7299.
18 X.C. Wang, K. Maeda, A. Thomas, K. Takanabe, G. Xin, J.M. Carlsson, K. Domen and M. Antonietti, *Nat.Mater.*, 2009, **8**, 76–80.
19 K. Takanabe, K. Kamata, X. Wang, M. Antonietti, J. Kubota and K. Domen, *Phys. Chem. Chem. Phys.*, 2010, **12**, 13020–13025.
20 F. Dong, L.W. Wu, Y.J. Sun, M. Fu, Z.B.Wu and S.C. Lee, *J. Mater. Chem.*, 2011, **21** 15171–15174.
21 B. Chai, T.Y. Peng, J. Mao, K. Li and L. Zan, *Phys. Chem. Chem. Phys.*, 2012, **14**, 16745–16752.
22 J.H.Liu, Y.W. Zhang, L.H. Lu, G. Wu and W. Chen, *Chem. Commun.*, 2012, **48**, 8826–8828.
23 Y.W. Zhang, J.H. Liu, G. Wu and W. Chen, *Nanoscale* 2012, **4**, 5300–5303.
24 J.D. Hong, X.Y. Xia, Y.S. Wang and R. Xu, *J. Mater. Chem.*, 2012, **22**, 15006–15012
25 S.C. Yan, Z.S. Li and Z.G. Zou, *Langmuir*, 2010, **26**, 3894–3901.
26 S.C. Yan, Z.S. Li and Z.G. Zou, *Langmuir*, 2009, **25**, 10397–10401.
27 Y.J. Wang, Z.X. Wang, S. Muhammad and J. He, *CrystEngComm*, 2012, **14**, 5065–5070.
28 G.G. Zhang, J.S. Zhang, M.W. Zhang and X.C. Wang, *J. Mater. Chem.*, 2012, **22**, 8083–8091.
29 J.S. Zhang, M.W. Zhang, R.Q. Sun and X.C. Wang, *Angew. Chem. Int. Ed.*, 2012, **51**, 10145–10149.
30 S.C. Yan, S.B. Lv, Z.S. Li and Z.G. Zou, *Dalton Trans*., 2010, **39**, 1488–1491.
31 L. Ge, C.C. Han and J. Liu, *Appl. Catal. B:Environ.*, 2011, **108**, 100–107.
32 Q.J. Xiang, J.G. Yu, M. Jaroniec, *J. Phys. Chem. C*, 2011, **115**, 7355–7363.
33 F.Z. Su, S.C. Mathew, G. Lipner, X.Z. Fu and M. Antonietti, *J. Am. Chem. Soc.*, 2010, **132**, 16299–16301.
34 X.F. Chen, J.S. Zhang, X.Z. Fu, M. Antonietti and X.C. Wang, *J. Am. Chem. Soc.*, 2009, **131**, 11658–11659.
35 L. Ge, C.C. Han, J. Liu and Y.F. Li, *Appl. Catal. A: Gen.*, 2011, **409–410** ,215–222.
36 Y. Di, X.C. Wang, A. Thomas and M. Antonietti, *ChemCatChem*, 2010, **2**, 834–838.
37 C. Chang, Y. Fu, M. Hu, C.Y. Wang, G.Q. Shan and L.Y. Zhu. *Appl. Catal. B: Environ.*, 2013, **142-143**, 553– 560.
38 G. Liu, P. Niu, C. Sun, S.C. Smith, Z. Chen, G.Q. Lu and H.M. Cheng, *J. Am. Chem. Soc.*, 2010, **132**, 11642–11648.
39 S.C. Yan, Z.S. Li and Z.G. Zou, *Langmuir*,. 2010, **26,** 3894–3901.
40 Y.J. Zhang, T. Mori, J.H. Ye and M. Antonietti, *J. Am. Chem. Soc.*, 2010, **132**, 6294–6295.
41 H.J. Yan and H. Yan, *Chem. Commun.*, 2011, **47**, 4168–4170.
42 J. Fu, B.B. Chang, Y.L. Tian, F.N. Xi and X.P. Dong, *J. Mater. Chem. A*., 2013, **1**, 3083–3090.
43 Y.Y. Wang, X.J. Bai, C.S. Pan, J. He and Y.F. Zhu, *J. Mater. Chem.*, 2012, **22**, 11568–11573
44 D.L. Jiang, L.L. Chen, J.J. Zhu, M. Chen, W.D. Shi, and J.M. Xie, Dalton Trans., 2013, **42**, 15726-15734.
45 X.S. Zhou, B. Jin, L.D. Li, F. Peng, H.J. Wang, H. Yu and Y.P. Fang, *J. Mater. Chem.*, 2012, **22**, 17900–17905
46 W. Liu, M.L. Wang, C.X. Xu, S.F. Chen, *Chem. Eng. J.*, 2012, **209**, 386–393.
47 Y.J. Wang, Z.X. Wang, S. Muhammad and J. He, *CrystEngComm.*, 2012, **14**, 5065–5070.
48 H. McDaniel, P. E. Heil, C. L. Tsai, K. K. Kim and M. Shim, *ACS Nano*., 2011, **5**, 7677–7683.
49 M. Shim, H. McDaniel and N. Oh, *J. Phys. Chem. Lett.*, 2011, **2**, 2722–2727.
50 X.C. Wang, W.B. Mi, E.Y. Jiang and H.L. Bai, *Appl. Surf. Sci.*, 2009, **255**, 4005–4010.
51 S. C. Yan, S. B. Lv, Z. S. Li and Z. G. Zou, *Dalton Trans.*, 2010, **39**, 1488–1491.
52 S. Polarz, M. Antonietti, *Chem. Commun*. 2002, 2593–2604.
53 M. Groenewolt and M. Antonietti, *Adv. Mater.*, 2005, **17**, 1789–1792.
54 C. D. Liang, K. L. Hong, G. A. Guiochon, J. W. Mays and S. Dai, *Angew. Chem. Int. Ed.*, 2004, **116**, 5909–5913;
55 A. Thomas, F. Goettmann and M. Antonietti, *Chem. Mater*., 2008, **20**, 738–755.
56 M. Antonietti and C. Opin. *J. Colloid Interface Sci.*, 2001, **6**, 244–248.
57 D. H. Chen, Z. Li, Y. Wan, X. J. Tu, Y. F. Shi, Z. X. Chen, W. Shen, C. Z. Yu, B. Tu and D. Y. Zhao,*J. Mater. Chem.* 2006, **16**, 1511–1519.
58 C. D. Liang, Z. J. Li, S. Dai, *Angew. Chem. Int. Ed.*, 2008, **120**, 3754–3776.
59 N.Y. Cheng, J.Q. Tian, Q. Liu, C.J. Ge, A. H. Qusti, A. M. Asiri, A. O. Al-Youbi, and X.P. Sun, *Appl. Mater. Interfaces.*, 2013, **5**, 6815−6819.
60 Y. J. Zhang, A. Thomas, M. Antonietti and X. C. Wang, *J. Am. Chem. Soc.*,2009, **131**, 50–51.
61 Y.G. Xu,H. Xu, L. Wang, J. Yan, H.M. Li, Y.H. Song, L.Y. Huang and G.B. Cai, *Dalton Trans.*, 2013, **42**, 7604–7613
62 Y. Wang, Y. Di, M. Antonietti, H. R. Li, X. F. Chen and X. C. Wang, *Chem. Mater.*, 2010, **22**, 5119 –5121.
63 Y. Wang, H. R. Li, J. Yao, X. C. Wang and M. Antonietti, *Chem. Sci.*2011, **2**, 446–450.
64 G. Liu, P. Niu, C. H. Sun, S. C. Smith, Z. G. Chen, G. Q. Lu and H. M. Cheng, *J. Am. Chem. Soc.*, 2010, **132**, 11642–11648.
65 M. Kawaguchi and K. Nozaki, *Chem. Mater.*, 1995, **7**, 257–264.
66 J. S. Zhang, X. F. Chen, K. Takanabe, K. Maeda, K. Domen, J. D. Epping, X. Z. Fu, M. Antonietti and X. C. Wang, *Angew. Chem. Int. Ed.*, 2010, **122**, 451–454.
67 Geim, A. K., Novoselov and K. S, *Nat. Mater.*, 2007, **6**, 183–191.
68 Geim, A. K, *Science*., 2009, **324**, 1530–1534.
69 M. J. Allen, V. C. Tung and R. B. Kaner, *Chem. Rev.*,2010, **110**,132–145.
70 Y. Q. Sun, C. Li, Y. X. Xu, H. Bai, Z. Y. Yao and G. Q. Shi, *Chem. Commun.*, 2010, **46**, 4740–4742.
71 J. G. Yu, L. F. Qi and M. Jaroniec, *J. Phys. Chem. C.*, 2010,**114**, 13118–13125.
72 J. G. Yu, G. P. Dai and B. B. Huang, *J. Phys. Chem. C.*, 2009, **113,**16394–16401.
73 G. Williams, B. Seger and P. V. Kamat, *ACS Nano*, 2008, **2**, 1487–1491.
74 Y.B. Li, H.M. Zhang, P.R. Liu, D.Wang, Y. Li and H.J. Zhao, *Small*, 2013, **9**, 3336–3344.

75 W.J. Wang, J.C. Yu, D.H. Xia, P.K. Wong and Y.C. Li, *Environ. Sci. Technol*. 2013, **47**, 8724−8732.

76 L. Ge and C.C. Han, *Appl.Catal.B:Environ.*, 2012, **117– 118**, 268–274.

77 Y. G. Xu, H. Xu, L. Wang, J. Yan, H.M. Li, Y.H. Song, L.Y. Huang and G.B. Cai, *Dalton Trans.*, 2013, **42**, 7604–7613

78 Y. Sui, J.H. Liu, Y.W. Zhang, X.K. Tian and W. Chen, *Nanoscale*, 2013, **5**, 9150–9155.

79 Y.P. Yuan, S.W. Cao, Y.S. Liao, L.S. Yin and C. Xue, *Appl. Catal. B: Environ.*, 2013, **140-141**,164–168.

80 J.S. Zhang, M.W. Zhang, R.Q. Sun and X.C. Wang, *Angew. Chem. Int. Ed*.; 2012, **124**, 10292–10296.

81 F. Dong, Z.W. Zhao, T. Xiong, Z.L. Ni, W.D. Zhang, Y.J. Sun and W.K. Ho, *ACS Appl. Mater. Interfaces*, 2013, **5**, 11392–11401.

82 B. Chai, X. Liao, F.K. Song and H. Zhou, *Dalton Trans.*, 2014, **43**, 982–989.

83 S.S. Zhao, S. Chen, H.T. Yu and X. Quan, *Sep Purif. Technol*., 2012, **99**, 50–54.

84 K. Sridharan, E. Jang and T. J. Park, *Appl. Catal. B: Environ.*, 2013,**142– 143**, 718–728.

85 J.G. Yu, S.H. Wang, J.X. Low and W. Xiao, *Phys. Chem. Chem. Phys*., 2013, **15**, 16883–16890.

86 J. Ran, J. Yu and M. Jaroniec, *Green Chem.*, 2011, **13**, 2708–2713.

87 L. A. Silva, S. Y. Ryu, J. Choi, W. Choi and M. R. Hoffmann, *J. Phys. Chem. C*., 2008, **112**, 12069–12073.

88 Y.P. Zang, L.P. Li, Y. Zuo, H.F. Lin, G.S. Li and X.F. Guan, *RSC Adv.*, 2013, **3**, 13646–13650.

89 L.Y. Huang, H. Xu, Y.P. Li, H.M. Li, X.N. Cheng, J.X. Xia, Y.G. Xu and G.B. Cai, *Dalton Trans.*, 2013,**42**, 8606–8616.

90 K. Katsumata, R. Motoyoshi, N. Matsushita and K.Okada, *J. Hazard. Mater.*, 2013, **260**, 475– 482.

91 L. Xu, J.X. Xia, H. Xu, S. Yin, K. Wang, L.Y. Huang, L.G. Wang and H.M. Li, *J. Power Sources*., 2014, **245**, 866–874.

92 S. Ye, L. G. Qiu, Y.P. Yuan,Y.J. Zhu, J. Xia and J.F. Zhu, *J. Mater. Chem. A.*, 2013, **1**, 3008–3015.

93 L.Y. Huang,Y.P. Li, H. Xu,Y.G. Xu, J.X. Xia, K. Wang, H.M. Li and X.N. Cheng, *RSC Adv.*, 2013, **3**, 22269–22279.

94 L.Y. Huang, H. Xu, R.X. Zhang, X.N. Cheng, J.X. Xia,Y.G. Xu and H.M. Li, *Appl. Surf. Sci.*, 2013, **283**, 25-32.

95 X.S. Zhou, B. Jin, R.Q. Chen, F. Peng and Y.P. Fang, *Mater. Res. Bull.*, 2013, **48**, 1447–1452.

96 J.G. Yu, S.H. Wang, B. Cheng, Z. Lin and F. Huang, *Catal. Sci.* Technol., 2013, **3**, 1782–1789.

97 M. Xu, L. Han, and S.H. Dong, *ACS Appl. Mater. Interfaces.*, 2013, **5**, 12533–12540

98 Y.D. Hou, A. B. Laursen, J.S. Zhang, G.G. Zhang, Y.S. Zhu and X.C. Wang, *Angew. Chem. Int. Ed.*. 2013, **52**, 3621-3625..

99 J.D. Hong, Y.S. Wang, Y.B. Wang, W. Zhang and R. Xu, ChemSusChem,. 2013, **6**, 2263–2268.

100 J.X. Sun, Y.P. Yuan, L.G. Qiu, X. Jiang, A.J. Xie, Y.H. Shen and J.F. Zhu, *Dalton Trans.*, 2012, **41**, 6756–6763.

101 W. Liu, M.L. Wang, C.X. Xu and S.f. Chen, *Chem. Eng. J*. 2012, **209**, 386–393.

102 S.W. Cao, X. F. Liu, Y.P. Yuan, Z.Y. Zhang, Y.S. Liao, J. Fang, S. .C.J. Loo, T. C. Sum and C.Xue, *Appl. Catal. B: Environ.*, 2014, **147**, 940–946.

103 Z.Y. Jin, N.Y. Murakami, T. Tsubota, T. Ohno, *Appl. Catal. B: Environ.*, 2014, **150-151** , 479–485.

104 M. Shalom, S. Inal, D.Neherb, M. Antonietti, *Catal. Taday*. 2014, **225**, 185-190.

105 Y.J. Wang, X.J. Bai, C.S. Pan, J. He and Y.F. Zhu, *J. Mater. Chem*., 2012, **22**, 11568–11573.

106 Y.L. Tian, B.B. Chang, J.L. Lu, J. Fu, F.N. Xi, and X.P. Dong, *ACS Appl. Mater. Inter.* 2013, **5**, 7079–7085.

107 T.T. Li, L.H. Zhao, Y.M. He, J. Cai, M.F. Luo and J.J. Lin, *Appl. Catal. B: Environ.*, 2013, **129**, 255–263.

108 M.W. Kanan, and D.G. Nocera, *Science.*, 2008, **321,** 1072–1075.

109 E.M.P. Steinmiller and K.S. Choi, *P. Natl. Acad. Sci.USA.*, 2009, **106**, 20633–20636.

110 Y. Surendranath, M. Dinca and D.G. Nocera, *J. Am. Chem. Soc.*, 2009, **131**, 2615–2620.

111 D.A. Lutterman, Y. Surendranath and D.G. Nocera, *J. Am. Chem. Soc.*, 2009, **131**, 3838–3839.

112 Y. Surendranath, D.A. Lutterman, Y. Liu and D.G. Nocera, *J. Am.Chem. Soc.*, 2012, **134**, 6326–6336.

113 L. Ge, C.C. Han, X.L. Xiao and L.L. Guo, *Appl.Catal.B:Environ.*, 2013,**142–143**, 414–422.

114 Y.J. Wang, Z.X. Wang, S. Muhammad and J. He, *CrystEngComm*, 2012, **14**, 5065–5070.

115 S. Zhu, T. Xu, H. Fu, J. Zhao and Y. Zhu, *Environ. Sci. Technol*., 2007, **41**, 6234.

116 G. Yu, J. Gao, J. C. Hummelen, F. Wudl and A. J. Heeger, *Science*,.1995, **270**, 1789.

117 C.S. Pan, J. Xu , Y.J. Wang , D. Li and Y.F. Zhu, *Adv. Funct. Mater.*, 2012, **22**, 1518–1524.

118 F.J. Zhang, F.Z. Xie, S.F. Zhu, J. Liu, J. Zhang, S.F. Mei and W. Zhao, *Chem. Eng. J.*, 2013, **228**, 435–441.

119 S.Kumar, T. Surendar, A. Baruah and V. Shanker, *J. Mater. Chem. A.*, 2013, **1**, 5333–5340.

120 Y. Liu, G. Chen, C. Zhou, Y.D. Hu, D.G. Fu, J. Liu and Q. Wang, *J. Hazard. Mater.*, 2011, **190**, 75–80.

121 Y.M. He, J. Cai, T.T. Li, Y. Wu, H.J. Lin, L.H. Zhao and M.F. Luo, *Chem. Eng. J.*, 2013, **215-216,** 721–730.

122 S.Kumar, B. Kumar and S.T.V. Shanker, *Mater. Res. Bull*., 2014, **49**, 310–318.

123 H.W. Kang, S. N. Lim, D.S. Song and S. B. Park, *Int.J.Hydrogen.Energ.*, 2012, **37**, 11602–11610.

124 S.Q. Zhang, Y.X. Yang, Y.N. Guo, W. Guo, M. Wang, Y.H. Guo and M.X. Huo, *J. Hazard. Mater.*, 2013, **261**, 235–245.

125 S.M. Wang, D.L. Li, C. Sun, S.G. Yang, Y. Guan and H. He, *Appl.Catal.B:Environ.*, 2014, **144**, 885–892.

126 X. Zhang, Z. Ai, F. Jia and L. Zhang, *J. Phys. Chem. C.*, 2008, **112**, 747–753.

127 J. Henle, P. Simon, A. Frenzel, S. Scholz and S. Kaskel, *Chem. Mater.*, 2007, **19**, 366–373.

128 M.A. Gondala, X. Chang, M.A. Ali, Z.H. Yamania, Q. Zhou and G. Ji, *Appl. Catal. A-Gen.*, 2011, **397**,192–200.

129 L. Ye, J. Liu, C. Gong, L. Tian, T. Peng and L. Zan, *ACS Catal*., 2012, **2**, 1677–1683.

130 L. Ye, C. Gong, J. Liu, L. Tian, T. Peng, K. Deng and L. Zan, *J. Mater. Chem.*, 2012, **22**, 8354–8360.

131 L. Ye, L. Tian, T. Peng and L. Zan, *J. Mater. Chem.*, 2011, **21**, 12479–12484.

132 Y. Feng, L. Li, J. Li, J. Wang and L. Liu, *J. Hazard. Mater.*, 2011, **192**, 538–544.

133 Y. Fan, Y. Huang, J. Yang, P. Wang and G. Cheng, *Environ. Sci. Technol*., 2011, **45**, 1593–1600.

134 J. Xu, W. Meng, Y. Zhang, L. Li and C. Guo, *Appl.Catal.B:Environ.*, 2011, **107**, 355–362.

135 W.L. Huang, Q. Zhu, *Comp. Mater. Sci.*, 2008, **43**, 1101–1108.

136 L. Ye, L. Zan, L. Tian, T. Peng and J. Zhang, Chem. Commun. 2011, **47**, 6951–6953.

137 J. Jiang, K. Zhao, X. Xiao, L. Zhang, *J. Am. Chem.Soc.* 2012, **134**, 4473–4476.

138 L.Q. Ye, J.Y. Liu, Z. Jiang, T.Y. Peng and L. Zan, *Appl. Catal. B: Environ.*, 2013, **142-143**,1–7.

139 Y.J. Sun, W.D. Zhang, T. Xiong, Z.W. Zhao, F. Dong, R.Q. Wang and W.K. Ho, *J. Colloid Interface. Sci.*, 2014, **418**, 317–323.

140 D.L. Jiang, L.l. Chen, J.J. Zhu, M. Chen, W.D. Shi and J.M. Xie, *Dalton Trans.*, 2013, **42**, 15726–15734.

141 X.J. Wang, Q. Wang, F.T. Li, W.Y. Yang and Y. Zhao, *Chem. Eng. J*., 2013, **234**, 361-371.

142 H. Wang, J. Gao, T. Guo, R. Wang, L. Guo, Y. Liu and J. Li, *Chem.Commun.*, 2012, **48** 275–277.

143 Z. Lou, B. Huang, X. Qin, X. Zhang, Z. Wang Z. Zheng, H. Cheng, P. Wang and Y. Dai, *Catal. Today.*, 2011, **175**, 256–263.

144 L. Liu, H. Xu, H. Li, Y. Xu, J. Xia and S. Yin, *J.Phys.Chem.Solids*., 2012, **73**, 523–529.

145 H.Xu, J. Yan, Y.G. Xu, Y.H. Song, H.M. Li, J.X. Xia, C.J. Huang and H.L.Wan, *Appl. Catal. B: Environ.*, **129**,182–193.

146 C.R. Crowell and S.M. Sze, *solid-state electronics*,1966, **9**, 1035-1048.

147 Y. Di, X.C. Wang, A. Thomas and M. Antonietti, *ChemCatChem*, 2010, **2**, 834-838

148 J. S. Jang, H. G. Kim and J. S. Lee, *Catal. Today*, 2012, **185**, 270–277.

149 P. V. Kamat, *J. Phys. Chem. Lett.*, 2012, **3** (5), 663–672.

150 N. Serpone, A.V. Emeline, *J. Phys. Chem. Lett.*2012, **3**, 673−677

151 K.Y. Lee, R. Hahn, M. Altomare,E. Selli and P. Schmuki, *Adv. Mater.*2013, **25**, 6133–6137

152 H. Chen , S. Chen , X. Quan , H.T. Yu ,H.M. Zhao and Y.B. Zhang, *J. Phys. Chem. C*, 2008, **112** (25), 9285–9290.

153 S. Mubeen, J. Lee, N. Singh, S. Krämer, G. D. Stucky and M.Moskovits, *Nat. Nanotechnol*, 2013, **8**, 247–251

154 S. N.Basahel, K.Y.Lee, R.Hahn, P.Schmuki, S.M.Bawakeda and S.A. Al-Thabaiti, Chem. Commun. 2014, **48**, 6123-6125.

155 Y. Di, X.C. Wang, A. Thomas and M. Antonietti, *ChemCatChem*, 2010, **2**, 834 – 838.

156 H.Y. Zhu, X. Chen, Z.F. Zheng, X.B. Ke , E. Jaatinen, J.C. Zhao, C. Guo, T.F. Xie and D.J. Wang, *Chem. Commun.*,2009, 7524−7526.

157 N.Y. Cheng, J.Q. Tian, Q. Liu, C.J. Ge, A. H. Qusti, A. M. Asiri, A. O. Al-Youbi and X.P. Sun, *ACS Appl. Mater. Interfaces*., 2013, **5**, 6815−6819.

158 Y.X. Yang, Y.N. Guo, F.Y. Liu, X. Yuan, Y.H. Guo, S.Q. Zhang, W. Guo and M.X. Huo, *Appl. Catal. B: Environ.*, 2013, **142– 143**, 828– 837.

159 X.J. Bai, R.L. Zong, C.X. Li, D. Liu, Y.F. Liu and Y.F. Zhu, *Appl. Catal. B: Environ.*, 2014, **147**, 82–91.

160 C. Chang, Y. Fu, M. Hu, C.y. Wang, G.q. Shan and L.Y. Zhu, *Appl. Catal. B: Environ.*, 2013,**142–143**, 553–560.

161 X.H.Li, X.C.Wang and M. Antonietti, *Chem. Sci.*, 2012, **3**, 2170–2174.

162 D.B. Ingram, P. Christopher, J.L. Bauer and S. Linic, *ACS Catalysis.*, 2011, **1**, 1441–1447.

163 S.W. Cao, Z. Yin, J. Barber, F.Y.C. Boey, S.C.J. Loo, C. Xue, *ACS Appl. Mater. Interfaces*., 2011, **4** , 418–423.

164 J. Cao, Y.J. Zhao, H.L. Lin, B.Y. Xu and S.F. Chen, *Mater. Res. Bull.*, 2013, **48**, 3873–3880.

165 B. Chai, T.Y. Peng, J. Mao, K. Li and L. Zan, *Phys. Chem. Chem. Phys.*, 2012, **14**, 16745–16752.

166 S. Obregón and G. Colón, *Appl.Catal.B:Environ.*, 2014, **144** ,775–782.

167 J.T. Jin, X.G. Fu,Qiao Liu and J.Y. Zhang，*J. Mater. Chem. A.*, 2013, **1**, 10538–10545.

168 J.G. Yu, J.C. Yu, M. K. P. Leung, W. K. Ho, B. Cheng, X. J. Zhao and J. C. Zhao, *J. Catal.*, 2003, **217**, 69–78.

169 J.G. Yu, W.G. Wang, B. Cheng and B.L. Su, *J. Phys. Chem. C.*, 2009, **113**, 6743–6750.

170 J. G. Yu, L. J. Zhang, B. Cheng and Y. R. Su, *J. Phys. Chem. C*, 2007, **111**, 10582–10589.

171 J. C. Yu, W. K. Ho, J. G. Yu, H. Yip, P. K. Wong and J. C. Zhao, *Environ. Sci. Technol*. 2005, **39**, 1175–1179.

172 J. G. Yu, Y. R. Su and B. Cheng, *Adv. Funct. Mater.*, 2007, **17**, 1984–1990.

173 B. Cheng, Y. Le and J. G. Yu, *J. Hazard. Mater.*, 2010,**177**, 971–977.

174 J. G. Yu, G. P. Dai and B. B. Huang, *J. Phys. Chem. C*, 2009, **113**, 16394–16401.

175 J. G. Yu, Q. J. Xiang, J. R. Ran and S. Mann, *CrystEngComm*., 2010,**12**, 872–879.

176 W.D. Zhang,Y.J. Sun, F. Dong, W. Zhang, S. Duan and Q. Zhang, *Dalton Trans.*,2014,**43**, 12026–12036.

177 J. G. Yu and J. R. Ran, *Energy Environ. Sci*., 2011, **4**, 1364–1371.

178 J. G. Yu, Y. Hai and M. Jaroniec, *J. Colloid Interf.Sci*., 2011, **357**, 223–228.

179 H.J. Yan, Y. Chen, and S.M. Xu, *Int. J. Hydrogen. Energ*. 2012, **37**,125–133.

180 S.W. Cao, and J.G. Yu, *J. Phys. Chem. Lett*. 2014, **5**, 2101−2107.

181 S. Patchkovskii, J.S.Tse, S. N. Yurchenko, L. Zhechkov, T. Heine and G.Seifert, *P. Natl. Acad. Sci.USA*.,2005, **102**, 10439–10444.

182 S.C. Roy, O.K. Varghese, M. Paulose and C.A. Grimes, *ACS Nano*., 2010, **4**, 1259–1278.

183 H.F. Cheng, B.B. Huang, Y.Y. Liu, Z.Y. Wang, X.Y. Qin, X.Y. Zhang, Y. Dai, *Chem. Commun.* 2012, **48**, 9729–9731.

184 X.Y. Chen, Y. Zhou, Q. Liu, Z.D. Li, J.G. Liu and Z.G. Zou, *ACS Appl. Mater. Interfaces*., 2012, **4**,3372–3377.

185 H. Xu, S.X. Ouyang, P. Li, T. Kako and J.H. Ye, *ACS Appl. Mater. Interfaces*., 2013, **5**,1348–1354.

186 X.L. Liang, X. Dong, G.D. Lin and H.B. Zhang, *Appl. Catal. B: Environ.*, 2009, **88**, 315–322.